Supporting Information for:

A steric hindrance regulated probe with single excitation dual emissions for self-adaptive detection of biothiols and H_2S in human urine samples and living cells

Zhan Wang [b, #], Wenbo Shi [c #], Yi−Jun Gong [d, #], Yanjun Du [c], Wei Luo [a], Huang Zhou [a], and Ke Pan [a, *]

[a] Department of General Surgery, The Second Xiangya Hospital, Central South University, Changsha, China
[b] Department of Medical Oncology, Lung Cancer and Gastrointestinal Unit, Hunan Cancer Hospital/The Affiliated Cancer Hospital of Xiangya School of Medicine, Central South University, Changsha 410000, China.
[c] Department of Medical Oncology，Ruijin-Hainan Hospital, Shanghai Jiao Tong University School of Medicine, Qionghai City, Hainan Province, 571442, China.
[d] School of Chemistry and Chemical Engineering, Henan Normal University, Xinxiang, 453007, P. R. China
[#] co-first authors; [*] corresponding author: Email: panke@csu.edu.cn, gongyijun@htu.edu.cn

Table of Contents

1. Experimental procedures

Reagents and apparatus

All primary chemical reagents, including 2-Hydroxy acetophenone, 2,5,5-Trimethylcyclohexanone (isophorone), 3-Hydroxy-3-methyl-2-butonone, Malononitrile, 4-Hydroxybenzaldehyde, 3,5-Difluoro-4-hydroxybenzaldehyde, 4-Chloro-7-nitro-2,1,3-benzoxadiazole (NBD-Cl), *N*-Ethylmaleimide (NEM), and ultra dry solvents, are purchased from Energy Chemical (Shanghai, China). Ultrapure water from a Millipore Milli−Q water purification system (Billerica, MA, USA) for preparation of all aqueous solutions. The pH measurements were carried out with a Mettler−Toledo Delta 320 pH meter. Thin layer chromatography (TLC) analysis was performed on fluorescent thin-layer plates, and column chromatography was conducted over a silica gel (mesh 200−300). ^{1}H and ^{13}C NMR spectra were recorded using a Bruker DRX−600 or 400 spectrometer with chemical shifts reported as ppm (tetramethyl silane as internal standard). High resolution mass spectra (HRMS) were recorded using a Bruker MicroTOF−QII mass instrument (ESI). UV−vis absorption spectra and fluorescence intensity measurements were recorded using an Agilent Cary100 UV−Vis spectrophotometer and a Hitachi F7000 fluorescence spectrophotometer, respectively. Fluorescence images of cells were obtained using an Olympus FV1000−IX81 confocal laser scanning microscope (Japan).

Synthetic procedure

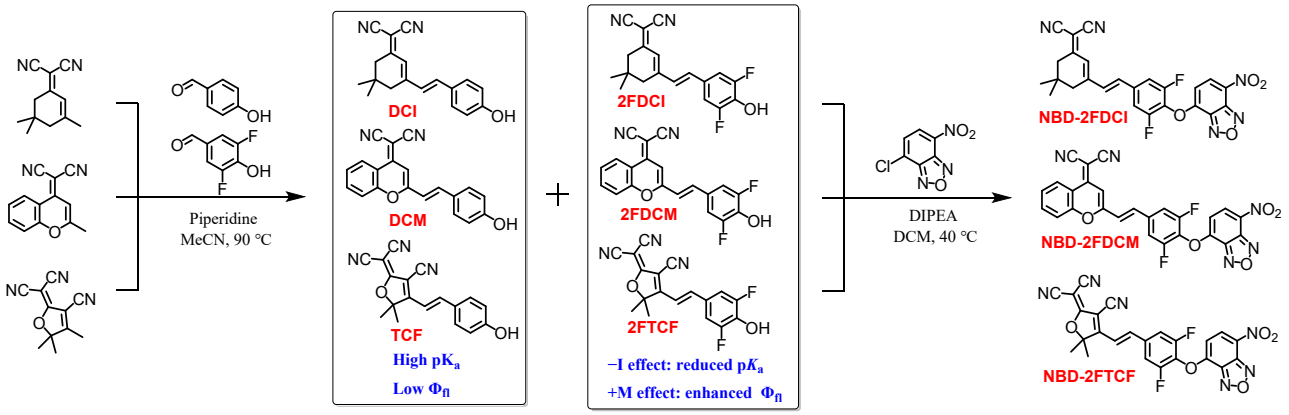

Scheme S1. The synthetic route.

General synthetic procedure for dyes: Dicyanomethylidene-1,5,5-trimethylcyclohexene (The electron withdrawing group DCI) [1], 4-(dicyanomethylene)-2-methylchromone (The electron withdrawing group DCM) [2], and 2-Dicyanomethylene-3-cyano-4,5,5-trimethyl-2,5-dihydrofuran (The electron withdrawing group TCF) [3] were synthesized according to the previous papers. All the hydroxyl functional dyes were synthesized according to the similar procedure. Briefly, the electron withdrawing group (DCI, DCM, or TCF, 11 mmol) and benzaldehyde (10 mmol) were dissolved in 20 mL acetonitrile with 10 drops piperidine as catalytic agent, and the mixture in opened round bottom flask was refluxed at 90 °C until the solvent was evaporated. The residue was purified by silica column chromatography.

DCI: DCI was purified using petroleum ether/dichloromethane (10:1 to 1:2, v/v) as an eluent to obtain a dark-red solid (2.32 g, 8.0 mmol, yield 80%). As DCI was a known compound,

characterization spectrum was not given.

2FDCI: 2FDCI was purified using petroleum ether/dichloromethane (10:1 to 1:2, v/v) as an eluent to obtain an orange solid (2.34 g, 7.2 mmol, yield 72%). ^{1}H NMR (600 MHz, $CDCl_3$): δ (ppm) 7.06 (d, J = 7.8 Hz, 2H), 6.90-6.81 (m, 3H), 2.60 (s, 2H), 2.44 (s, 2H), 1.08 (s, 6H). ^{13}C NMR (150 MHz, $CDCl_3$): δ (ppm) 169.44, 153.62, 151.72, 135.11, 128.69, 126.66, 123.49, 113.42, 112.65, 110.61, 78.47, 42.95, 39.15, 32.00, 27.92. HRMS (ESI) calcd for $C_{19}H_{16}F_2N_2O_1$ $[M - H]^-$ 325.1158, found 325.1148.

DCM: DCM was purified using dichloromethane/ethyl acetate (100:1 to 10:1, v/v) as an eluent to obtain a dark-red solid (1.84 g, 5.9 mmol, yield 59%). As DCM was a known compound, characterization spectrum was not given.

2FDCM: 2FDCM was purified using dichloromethane/ethyl acetate (100:1 to 10:1, v/v) as an eluent to obtain a yellow solid (2.02 g, 5.8 mmol, yield 58%). ^{1}H NMR (400 MHz, CD_3OD + DMSO-d_6): δ (ppm) 8.72 (d, J = 8.4 Hz, 1H), 7.78 (t, J = 8.0 Hz, 1H), 7.64 (d, J = 8.4 Hz, 1H), 7.52-7.44 (m, 2H), 7.32 (d, J = 9.2 Hz, 2H), 7.10 (d, J = 16.0 Hz, 1H), 6.84 (s, 1H). ^{13}C NMR (100 MHz, DMSO-d_6): δ (ppm) 158.26, 153.92, 153.13, 152.33, 151.52, 137.12, 135.90, 126.61, 125.06, 119.60, 119.36, 117.45, 116.21, 112.26, 112.04, 107.11, 60.76. HRMS (ESI) calcd for $C_{20}H_{10}F_2N_2O_2$ $[M - H]^-$ 347.0638, found 347.0631.

TCF: TCF was purified using dichloromethane/methanol (100:1, v/v) as an eluent to obtain a dark-red solid (2.03 g, 6.7 mmol, yield 67%). As TCF was a known compound, characterization spectrum was not given.

2FTCF: 2FTCF was purified using dichloromethane/methanol (100:1, v/v) as an eluent to obtain a brown solid (1.97 g, 5.8 mmol, yield 58%). ^{1}H NMR (400 MHz, CD_3OD + DMSO-d_6): δ (ppm) 7.85 (d, J = 16.4 Hz, 1H), 7.59-7.56 (m, 2H), 7.16 (d, J = 16.4 Hz, 1H), 1.85 (s, 6H). ^{13}C NMR (100 MHz, $CDCl_3$): δ (ppm) 176.73, 174.99, 153.78, 151.43, 145.59, 125.45, 114.69, 112.76, 112.05, 111.50, 110.56, 98.96, 55.40, 24.73. HRMS (ESI) calcd for $C_{18}H_{11}F_2N_3O_2$ $[M - H]^-$ 338.0747, found 338.0735.

Synthesis of probe NBD-2FDCI

The dye 2FDCI (326 mg, 1 mmol), NBD-Cl (220 mg, 1.1 mmol), and N,N-Diisopropylethylamine (DIPEA, 350 μL, 2 mmol) were dissolved in 20 mL dichloromethane, and the reaction was stirred at 40 °C until the color of the solution changed from purple to yellow. The residue was purified by silica column chromatography using dichloromethane as an eluent to obtain the probe NBD-2FDCI as a yellow solid (284 mg, yield 58%). ^{1}H NMR (600 MHz, $CDCl_3$): δ (ppm) 8.49 (d, J = 12.0 Hz, 1H), 7.27-7.25 (m, 2H), 7.02-6.90 (m, 3H), 6.72 (d, J = 12.0 Hz, 1H), 2.62 (s, 2H), 2.45 (s, 2H), 1.09 (s, 6H). ^{13}C NMR (150 MHz, $CDCl_3$): δ (ppm) 167.82, 155.49, 152.93, 150.90, 150.69, 143.37, 143.13, 135.24, 131.69, 131.04, 124.53, 111.96, 111.24, 110.65, 110.43, 107.37, 79.75, 41.92, 38.19, 31.08, 26.98. HRMS (ESI) calcd for $C_{25}H_{17}F_2N_5O_4$ $[M - H]^-$ 488.1176, found 488.1174.

Synthesis of probe NBD-2FDCM

The dye 2FDCM (348 mg, 1 mmol), NBD-Cl (220 mg, 1.1 mmol), and N,N-Diisopropylethylamine (DIPEA, 350 μL, 2 mmol) were dissolved in 20 mL dichloromethane, and the reaction was stirred at room temperature until the color of the solution changed from purple to orange. The residue was purified by silica column chromatography using dichloromethane as an eluent to obtain the probe NBD-2FDCM as a yellow solid (383 mg, yield 75%). ^{1}H NMR (600 MHz, CD_3OD + DMSO-d_6): δ (ppm) 8.97 (d, J = 8.4 Hz, 1H), 8.79 (d, J = 7.8 Hz, 1H), 8.12-8.08 (m, 2H), 8.01 (d, J = 8.4 Hz, 2H), 7.94-7.91 (m, 2H), 7.79-7.76 (m, 2H). 7.24 (d, J = 9.0 Hz, 1H). HRMS (ESI) calcd for $C_{26}H_{11}F_2N_6O_8$ $[M + NO_3]^-$ 573.0612, found 573.0604.

Synthesis of probe NBD-2FTCF

The dye 2FTCF (339 mg, 1 mmol), NBD-Cl (220 mg, 1.1 mmol), and N,N-Diisopropylethylamine (DIPEA, 350 μL, 2 mmol) were dissolved in 10 mL N,N-dimethylformamide, and the reaction was stirred at 40 °C for about 1 h until the color of the solution changed from blue to green. The mixture was diluted with 200 mL dichloromethane, washed with water and brine, and dried over anhydrous sodium sulfate. The organic phase was purified by silica column chromatography using dichloromethane/ethyl acetate (30:1 to 5:1, v/v) as an eluent to afford the probe NBD-2FTCF as a yellow solid (220 mg, yield 44%). ^{1}H NMR (600 MHz, $CDCl_3$ + CD_3OD): δ (ppm) 8.63 (d, J = 8.4 Hz, 1H), 7.87 (d, J = 16.4 Hz, 1H), 7.72 (d, J = 8.4 Hz, 2H), 7.27 (d, J = 16.4 Hz, 1H), 6.94 (d, J = 8.4 Hz, 1H). ^{13}C NMR (150 MHz, CD_3OD + DMSO-d_6): δ (ppm) 177.64, 175.00, 156.70, 155.04, 151.44, 145.47, 144.03, 136.04, 135.22, 133.19, 119.68, 114.88, 113.22, 112.48, 111.34, 110.81, 102.77, 100.48, 57.05, 25.76. HRMS (ESI) calcd for $C_{24}H_{11}F_2N_6O_5$ $[M - H]^-$ 501.0764, found 501.0778.

Computational methods.

All calculations were performed by Gaussian 09 program package. To study the ground state and excited geometries and the electron transitions involved in the absorption and emission, density functional theory (DFT) and time-dependent (TD)DFT theoretical calculations on the molecules were conducted. Geometries of ground and excited states were optimized without symmetry restriction by adopting B3LYP functional with 6-31+G(d) basis set. The calculations of the excitation were performed by the TDDFT method at B3LYP/6-31+G(d) level. The solvent effect was considered for TDDFT calculations by SMD model in water.

Determination of total biothiols in human urine by the Ellman method.

The total biothiols in human urine were measured by the Ellman method (UV-visible spectrophotometry). The thiols can react with 5,5'-dithiobis-(2-nitrobenzoic acid) (DTNB) to generate 2-nitro-5-thiobenzoic acid with yellow color and characteristic absorption peak at 412 nm, and the total thiol content can be quantitatively detected by the absorption changing. Briefly, the 5-fold diluted urine acted with or without DTNB were set as the sample group or the control group, the Cys solutions acted with or without DTNB were set as the standard group or the blank group. After incubation, absorbance at 412 nm of each group was determined via UV-Vis spectrophotometer, and the real absorbance was calculated using the following formulae: $\Delta A_{Sample} = A_{Sample} - A_{Control}$, $\Delta A_{Standard} = A_{Standard} - A_{Blank}$. The linear correlations of Ellman method was constructed according to the standard group with the Cys concentration range from 0 to 300 μM.

Determination of H_2S in human urine by WSP-5 probe.

The H_2S in human urine were measured by the commercial H_2S probe WSP-5. The probe can be degraded by H_2S to yield fluorescein with strong fluorescence at 525 nm, and the H_2S level can be quantitatively detected by the fluorescence intensity recovery. Briefly, the 5-fold diluted urine acted with or without WSP-5 were set as the sample group or the control group, the H_2S solutions acted with or without WSP-5 were set as the standard group or the blank group. After incubation, fluorescence intensity at 525 nm of each group was determined via fluorescence spectrophotometer, and the real intensity was calculated using the following formulae: $\Delta A_{Sample} = A_{Sample} - A_{Control}$, $\Delta A_{Standard} = A_{Standard} - A_{Blank}$. The linear correlations of WSP-5 was constructed according to the standard group with the H_2S concentration range from 0 to 100 μM.

Cytotoxicity assay

The cell cytotoxicities of 2FDCI and NBD-2FDCI were measured by the CCK-8 assay. Generally, HepG2 cells were cultured in a 96-well plates at 8×10^3 cells in 100 μL culture medium per well and incubated at 37 °C overnight. Then the medium was replaced with medium composed of 2, 5, 10, and 20 μM 2FDCI and NBD-2FDCI. After a 24 h incubation time, the cells were added with CCK-8 (10 μL) for 3 h. Microplate reader was used to determine the absorbance at 490 nm of each well, and the cell viability was evaluated according to the following formula: Cell viability ratio (%) = $(OD_{Sample} - OD_{PBS})/(OD_{Blank} - OD_{PBS}) \times 100\%$.

Reference

[1] Q.-Z. Li, J. Gu, Y.-C. Chen, Organocatalytic asymmetric [4 + 2] formal cycloadditions of cyclohexenylidenemalononitriles and enals to construct chiral bicyclo[2.2.2]octane, RSC Adv. 4 (2014) 37522−37525. https://doi.org/10.1039/C4RA07709A

[2] X. Zeng, Z. Chen, L. Tang, H. Yang, N. Liu, H. Zhou, Y. Li, J. Wu, Z. Deng, Y. Yu, H. Deng, X. Hong, Y. Xiao, A novel near-infrared fluorescent light-up probe for tumor imaging and drug-induced liver injury detection, Chem. Commun. 55 (2019) 2541−2544. https://doi.org/10.1039/C8CC10286D

[3] X. Yang, Z. Cai, D. Li, D. Lei, Y. Li, G. Wang, J. Zhang, X. Dou, D-π-A Dual-Mode Probe Design for the Detection of nM-Level Typical Oxidants, Anal. Chem. 94 (2022) 9184−9192. https://doi.org/10.1021/acs.analchem.2c01894

2. Supplementary figures

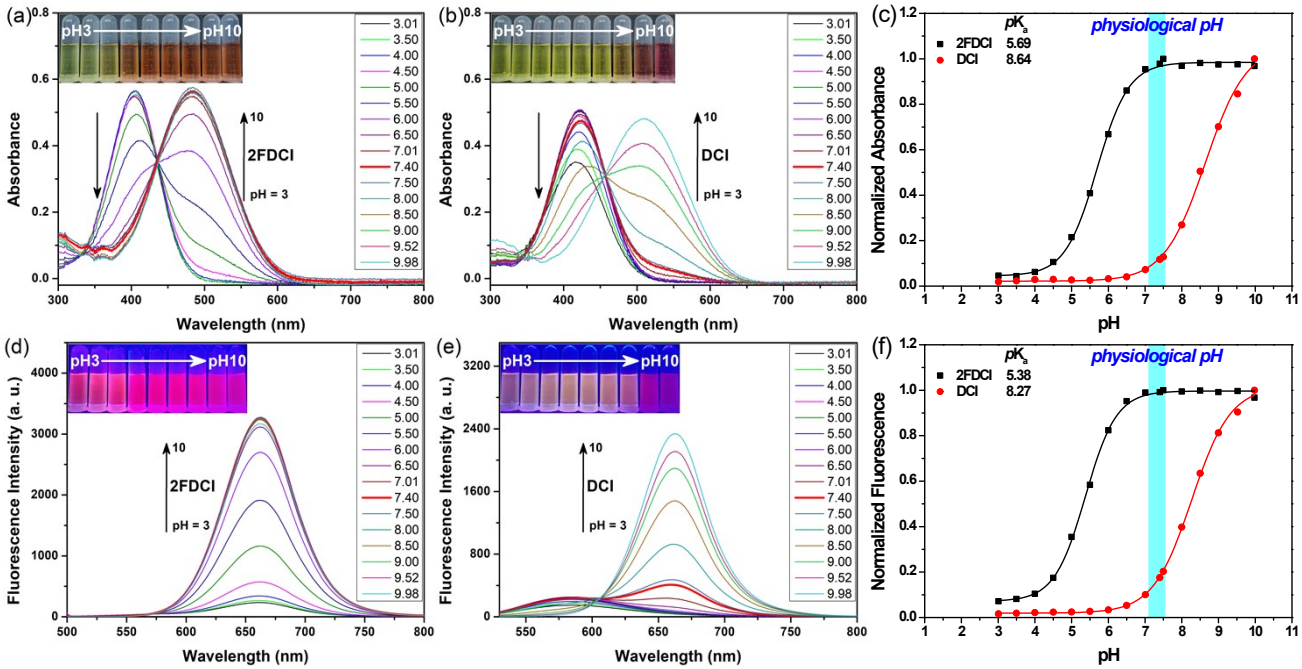

Figure S1. Absorption spectra of 20 μM **2FDCI** (a) and **DCI** (b) in various pH conditions (50 mM PBS, 20% EtOH as a co-solvent), insert: color changes of **2FDCI** and **DCI** from pH 3 to 10. (c) Normalized absorption responses of **2FDCI** and **DCI** at 483 nm and 509 nm toward pH value. (d) and **DCI** (e) in various pH conditions (50 mM PBS, 20% EtOH as a co-solvent), insert: fluorescence photos under 365 nm UV light of **2FDCI** and **DCI** from pH 3 to 10. (f) Normalized Fluorescence responses of **2FDCI** and **DCI** at 661 nm and 662 nm toward pH value.

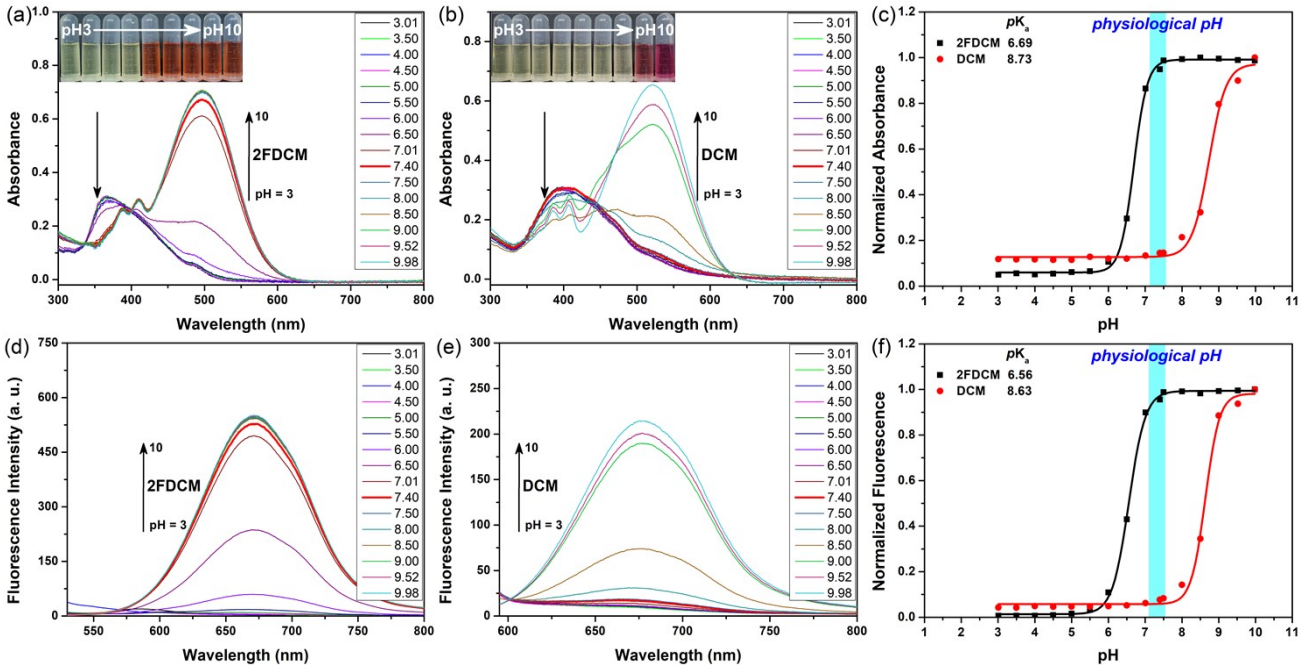

Figure S2. Absorption spectra of 20 μM **2FDCM** (a) and **DCM** (b) in various pH conditions (50 mM PBS, 20% EtOH as a co-solvent), insert: color changes of **2FDCM** and **DCM** from pH 3 to 10. (c) Absorption responses of **2FDCM** at 497 nm and **DCM** at 523 nm toward pH value. Fluorescence spectra of 20 μM **2FDCM** (d) and **DCM** (e) in various pH conditions (50 mM PBS, 20% EtOH as a co-solvent). (f) Fluorescence responses of **2FDCM** at 671 nm and **DCM** at 676 nm toward pH value.

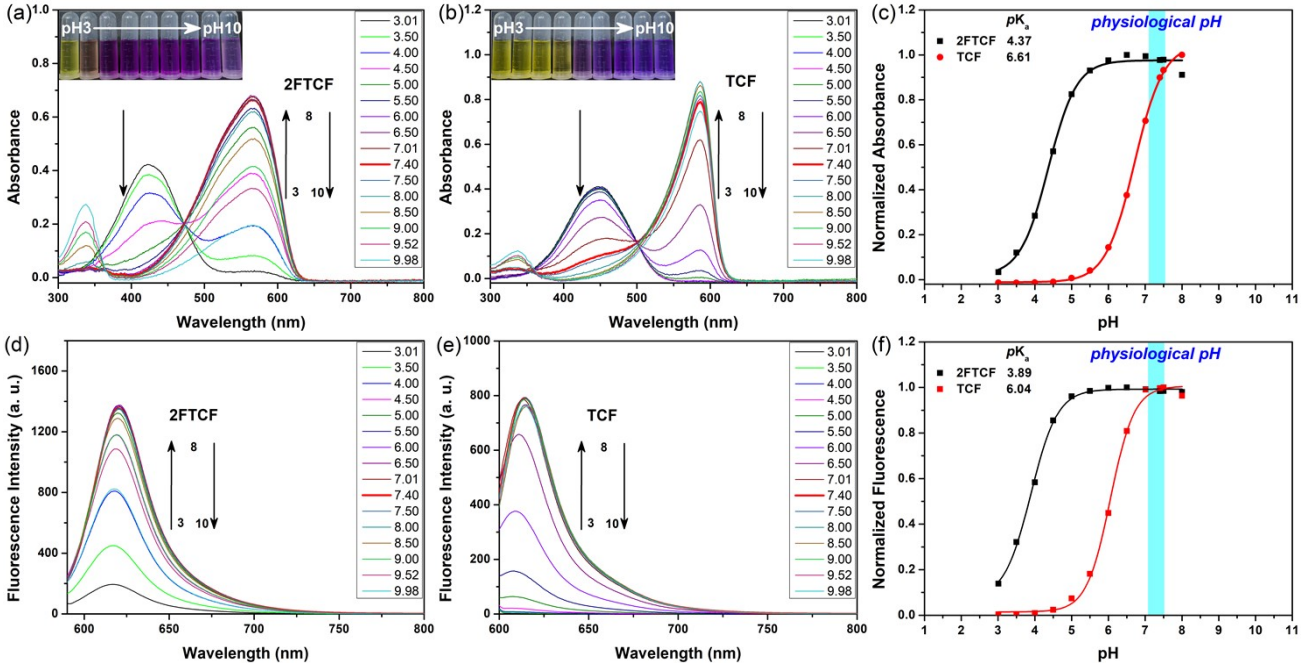

Figure S3. Absorption spectra of 20 μM **2FTCF** (a) and **TCF** (b) in various pH conditions (50 mM PBS, 20% EtOH as a co-solvent), insert: color changes of **2FTCF** and **TCF** from pH 3 to 10. (c) Absorption responses of **2FTCF** at 567 nm and **TCF** at 586 nm toward pH value. Fluorescence spectra of 20 μM **2FTCF** (d) and **TCF** (e) in various pH conditions (50 mM PBS, 20% EtOH as a co-solvent). (f) Fluorescence responses of **2FTCF** at 620 nm and **TCF** at 614 nm toward pH value.

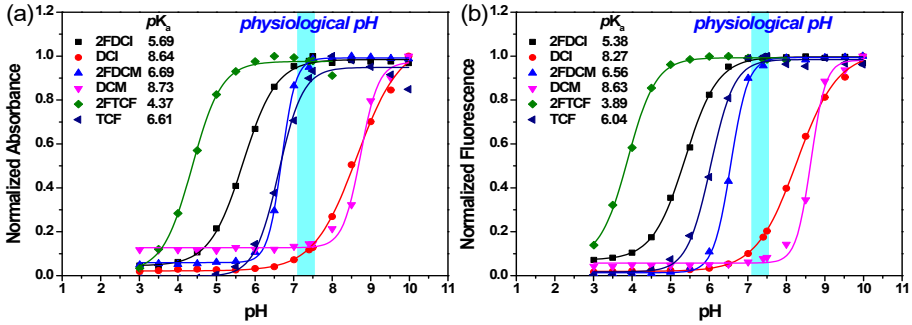

Figure S4. (a) Normalized absorption responses of **2FDCI**, **DCI**, **2FDCM**, **DCM**, **2FTCF**, and **TCF** at 483 nm, 509 nm, 497 nm, 523 nm, 567 nm, and 586 nm toward pH value, respectively. (b) Normalized fluorescence responses of **2FDCI**, **DCI**, **2FDCM**, **DCM**, **2FTCF**, and **TCF**, at 661 nm, 662 nm, 671 nm, 676 nm, 620 nm, and 614 nm toward pH value, respectively.

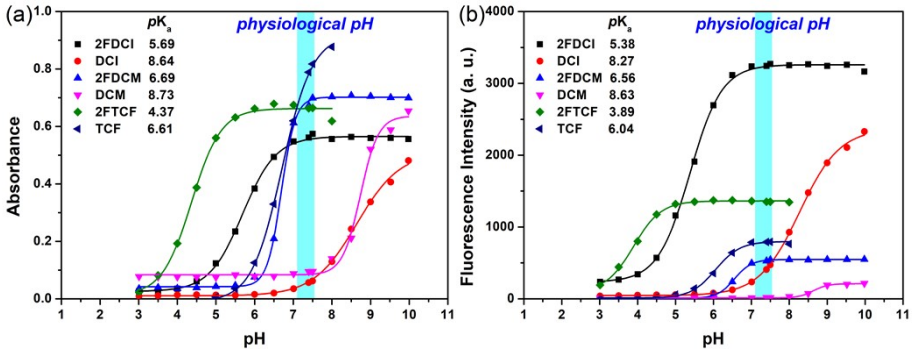

Figure S5. (a) Absorption responses of **2FDCI**, **DCI**, **2FDCM**, **DCM**, **2FTCF**, and **TCF**, at 483 nm, 509 nm, 497 nm, 523 nm, 567 nm, and 586 nm toward pH value, respectively. (b) Fluorescence responses of **2FDCI**, **DCI**, **2FDCM**, **DCM**, **2FTCF**, and **TCF**, at 661 nm, 662 nm, 671 nm, 676 nm, 620 nm, and 614 nm toward pH value, respectively.

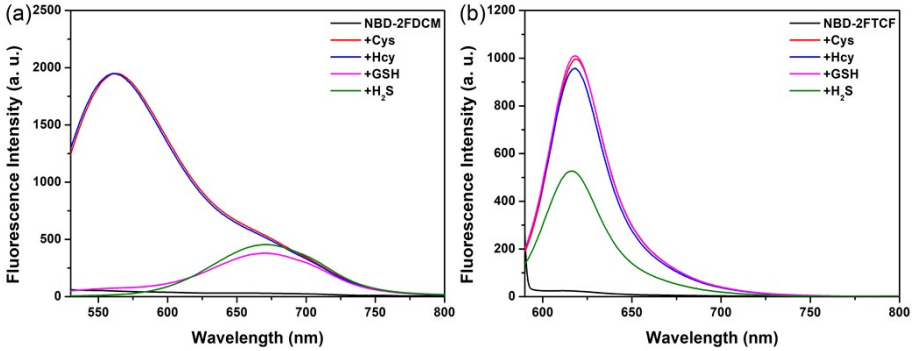

Figure S6. Fluorescence spectra of **NBD-2FDCM** (a) and **NBD-2FTCF** (b) in response to Cys, Hcy, GSH, and H_2S under excitation of 500 nm and 570 nm.

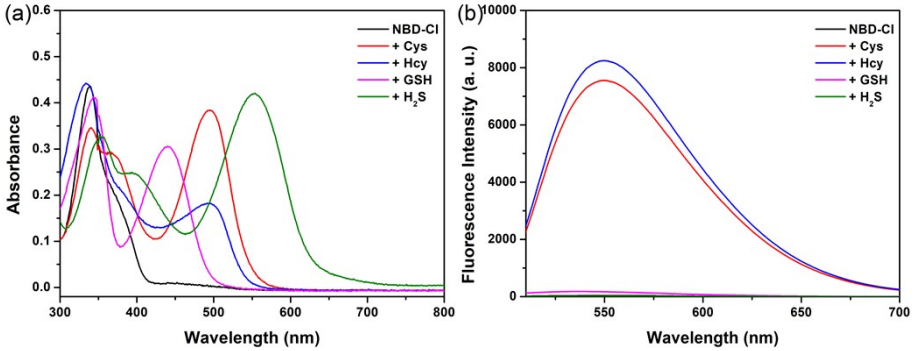

Figure S7. Absorption spectra of 15 μM **NBD-2FDCI** (a), **NBD-2FDCM** (c), and **NBD-2FTCF** (e) in response to Cys, Hcy, GSH, and H_2S, insert: color changes of **probes** in the present of analytes. Fluorescence spectra of 15 μM **NBD-2FDCI** (b), **NBD-2FDCM** (d), and **NBD-2FTCF** (f) in response to Cys, Hcy, GSH, and H_2S under excitation of 480 nm.

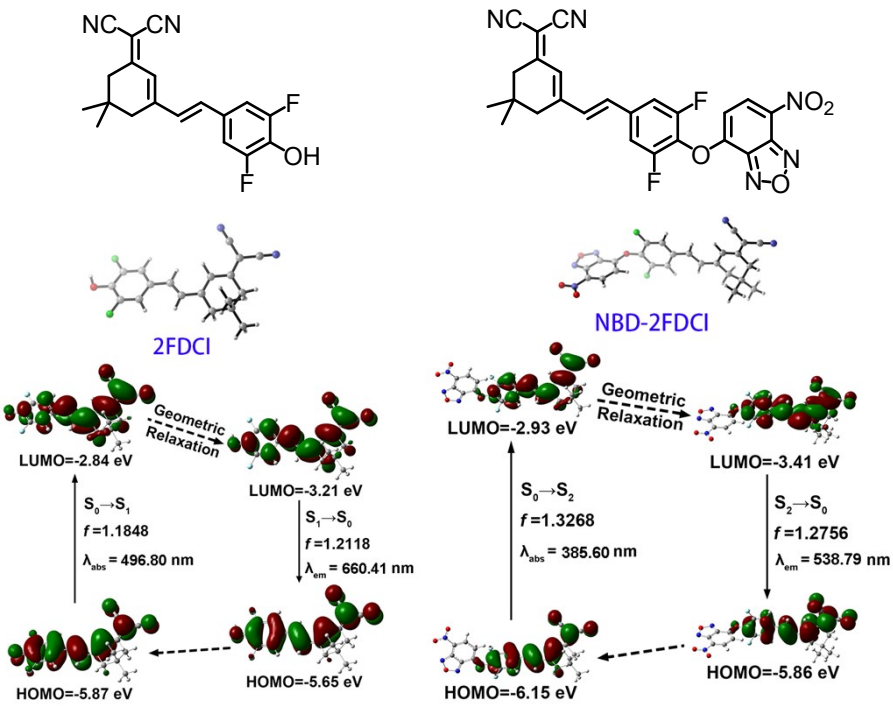

Figure S8. The HOMO and LUMO orbital energy of **2FDCI** and **NBD-2FDCI** using Gaussian 09 program package.

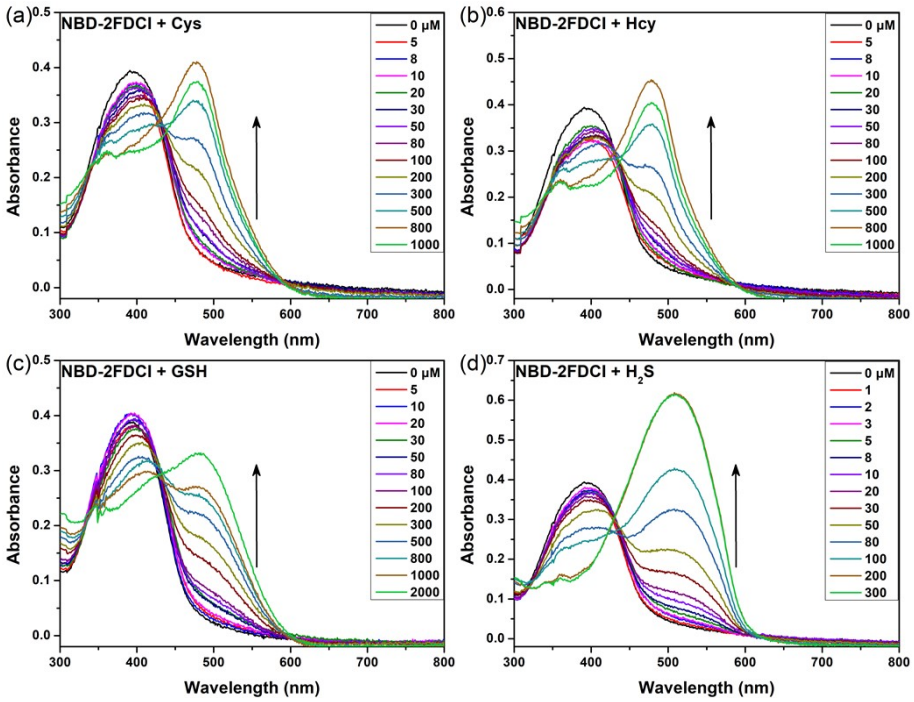

Figure S9. Absorption spectra of 15 μM **NBD-2FDCI** in response to Cys (a), Hcy (b), GSH (c), and H_2S (d) with concentrations of 5-1000 μM, 5-1000 μM, 5-2000 μM, and 1-300 μM, respectively.

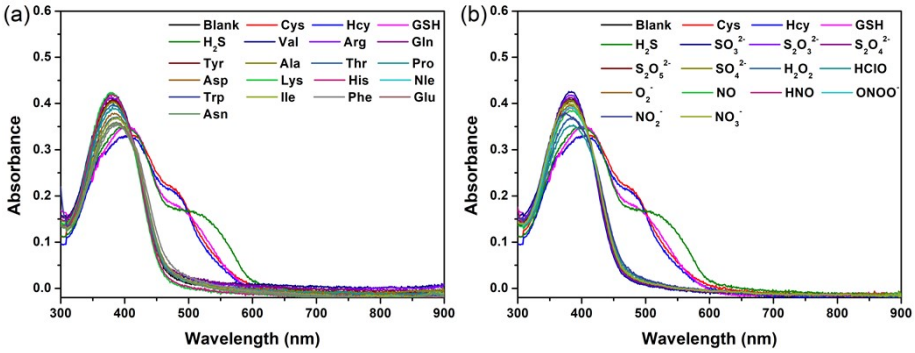

Figure S10. Absorption spectra of 15 μM **NBD-2FDCI** to 200 μM Cys, 200 μM Hcy, 300 μM GSH, and 30 μM H_2S, other common amino acid (a), or reactive species (b).

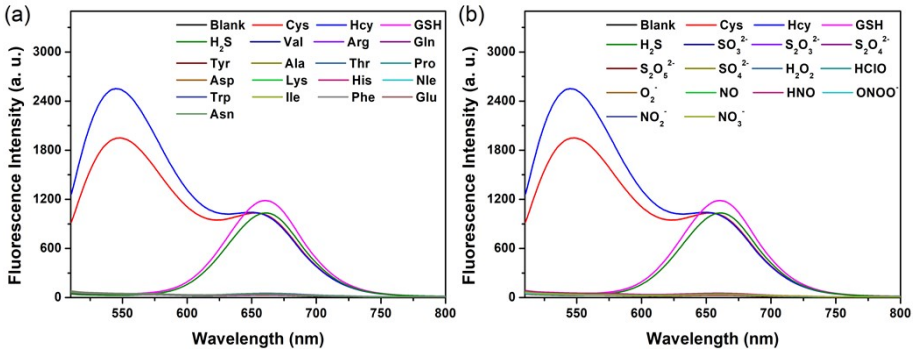

Figure S11. Fluorescence spectra of 15 μM **NBD-2FDCI** to 200 μM Cys, 200 μM Hcy, 300 μM GSH, and 30 μM H_2S, other common amino acid (a), or reactive species (b).

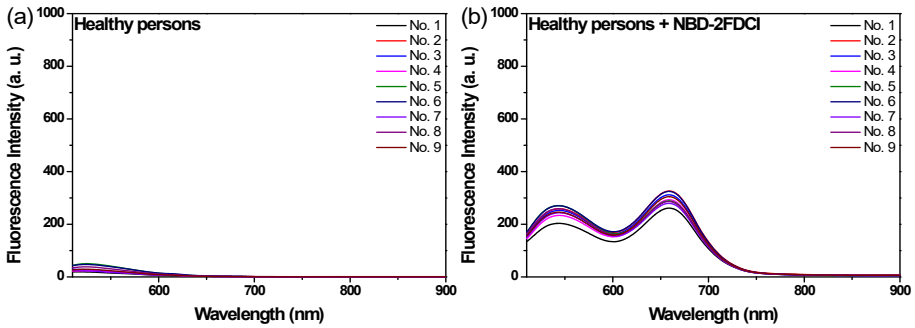

Figure S12. (a) Intrinsic fluorescence of 5-fold diluted human urine samples from healthy persons. (b) Fluorescence response results of probe probe **NBD-2FDCI** incubated with the urine samples in (a).

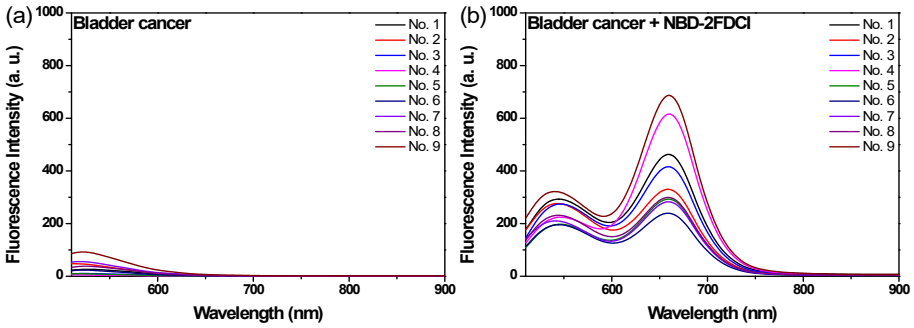

Figure S13. (a) Intrinsic fluorescence of 5-fold diluted human urine samples from bladder cancer patients. (b) Fluorescence response results of probe probe **NBD-2FDCI** incubated with the urine samples in (a).

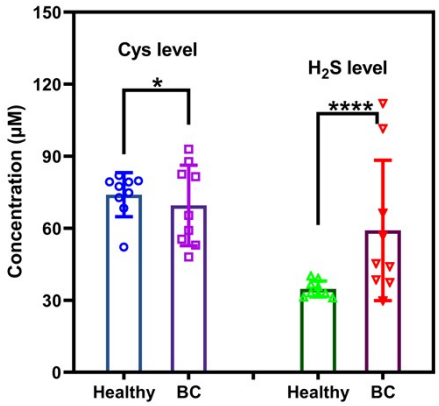

Figure S14. Quantification of Cys and H_2S with probe **NBD-2FDCI** in tris(2-carboxyethyl)phosphine (TCEP, a reducing agent) pretreated human urine samples of healthy persons and BC patients. Data denote mean ± s.d. (*P < 0.05, ****P < 0.0001).

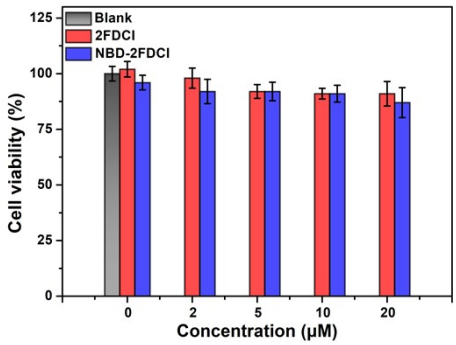

Figure S15. Cell viabilities of HepG2 cells treated with different concentrations of **2FDCI** and probe **NBD-2FDCI** for 24 hours.

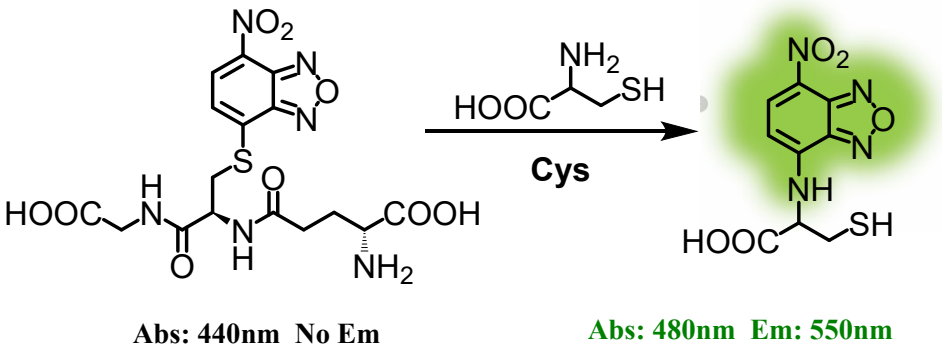

Scheme S2. Proposed response mechanism of the conversion of **NBD-GSH** to **NBD-Cys** in living cells.

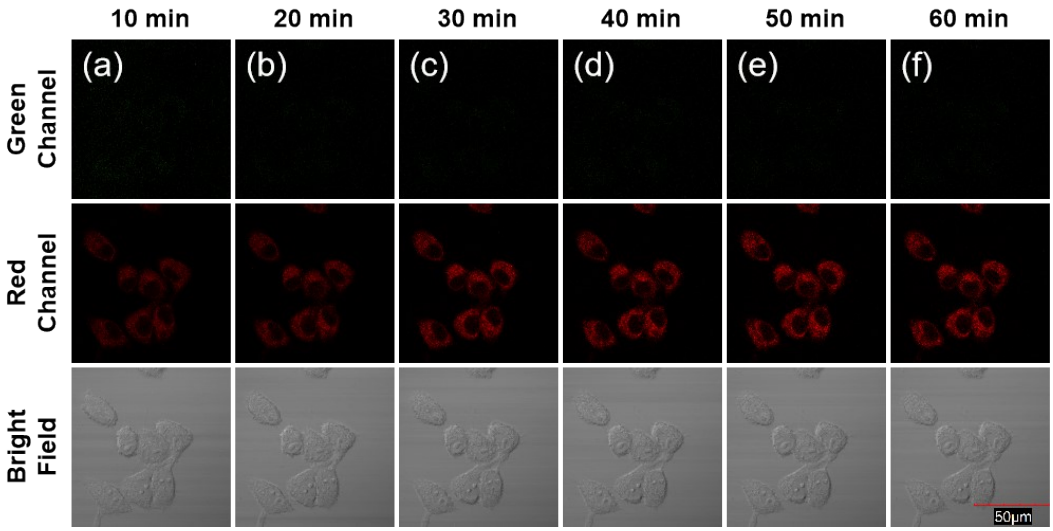

Figure S16. Time dependent fluorescence imaging of 500 μM GSH in 500 μM NEM pretreated HepG2 cells by 10 μM probe **NBD-2FDCI** staining. Excitation wavelength of 488 nm for both green channel (520-580 nm) and red channel (650-700 nm). Scale bars: 50 μm.

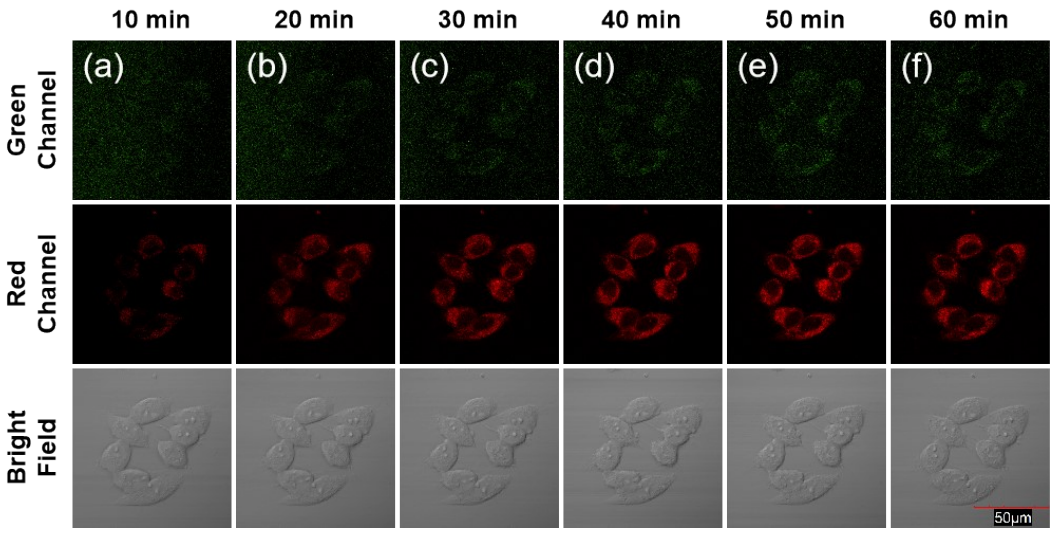

Figure S17. Time dependent fluorescence imaging of 200 μM Cys in 500 μM NEM pretreated HepG2 cells by 10 μM probe **NBD-2FDCI** staining. Excitation wavelength of 488 nm for both green channel (520-580 nm) and red channel (650-700 nm). Scale bars: 50 μm.

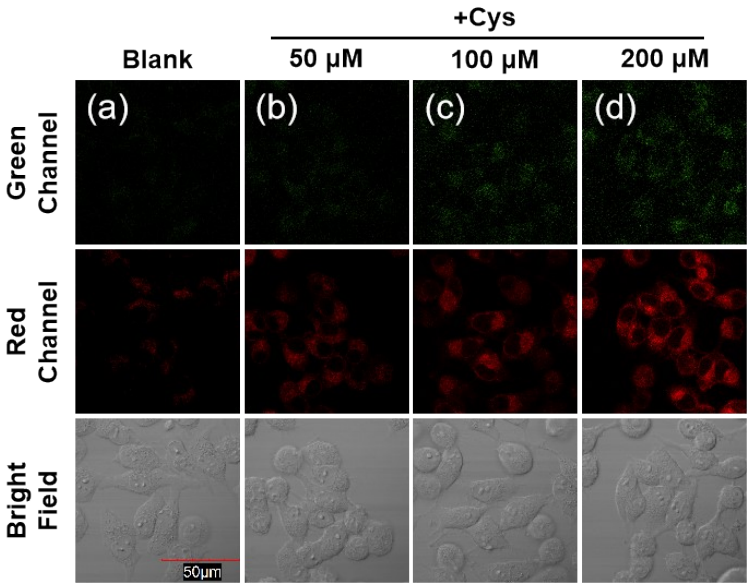

Figure S18. Fluorescence imaging of 50, 100, and 200 μM Cys in 500 μM NEM pretreated HepG2 cells by 10 μM probe **NBD-2FDCI** staining. Excitation wavelength of 488 nm for both green channel (520-580 nm) and red channel (650-700 nm). Scale bars: 50 μm.

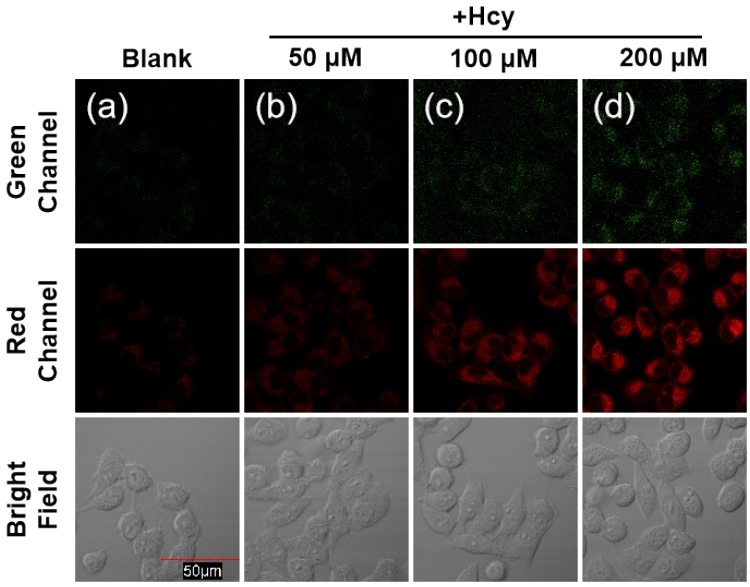

Figure S19. Fluorescence imaging of 50, 100, and 200 μM Hcy in 500 μM NEM pretreated HepG2 cells by 10 μM probe **NBD-2FDCI** staining. Excitation wavelength of 488 nm for both green channel (520-580 nm) and red channel (650-700 nm). Scale bars: 50 μm.

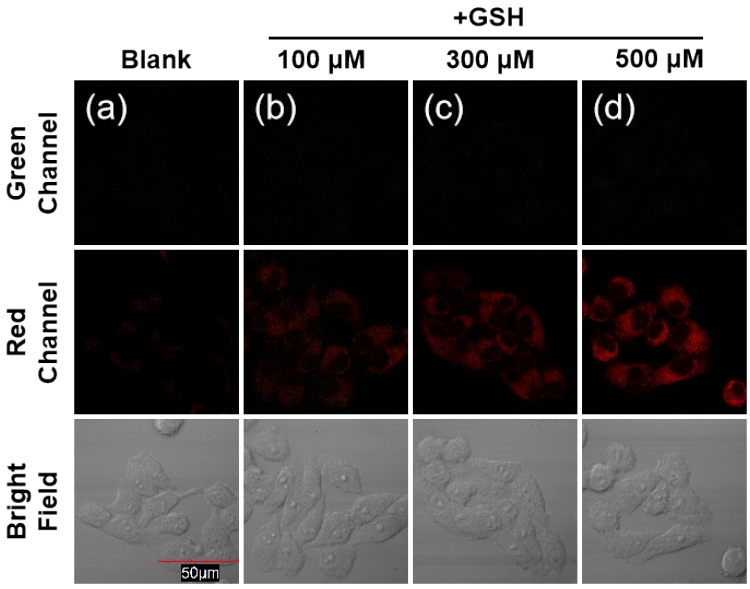

Figure S20. Fluorescence imaging of 100, 300, and 500 μM GSH in 500 μM NEM pretreated HepG2 cells by 10 μM probe **NBD-2FDCI** staining. Excitation wavelength of 488 nm for both green channel (520-580 nm) and red channel (650-700 nm). Scale bars: 50 μm.

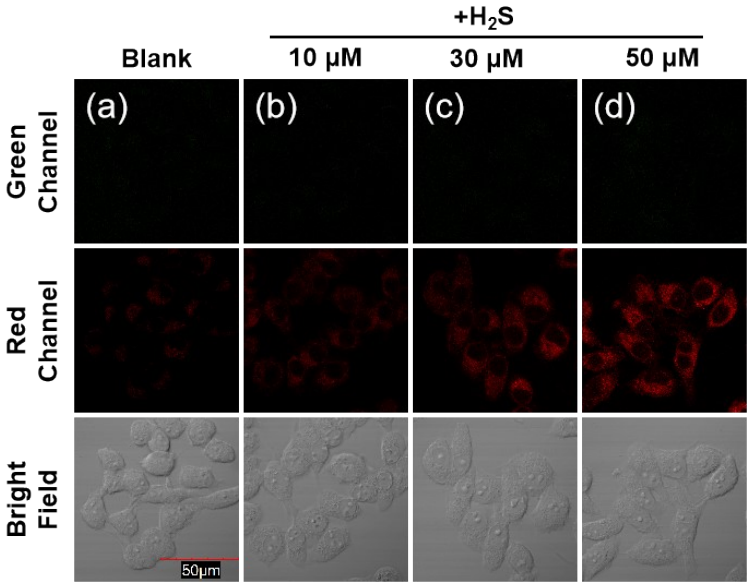

Figure S21. Fluorescence imaging of 10, 30, and 50 μM H_2S in 500 μM NEM pretreated HepG2 cells by 10 μM probe **NBD-2FDCI** staining. Excitation wavelength of 488 nm for both green channel (520-580 nm) and red channel (650-700 nm). Scale bars: 50 μm.

.

Table S1. Reported probes for biothiols and H_2S.

Probe	Analyte	$\lambda_{abs}/\lambda_{em}$ (nm)	LOD	Linear range	Response time	Enhance-ment	Applications
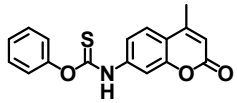 [1]	Cys	340/443	0.16 μM	0-35 μM	14 min	25-fold	Imaging in PC12 cells and living mouse brain
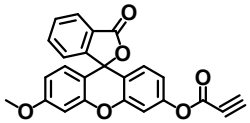 [2]	Cys	460/515	0.18 μM	0-100 μM	30 min	35-fold	Imaging in A549 cells
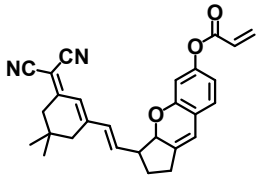 [3]	Cys	660/851	10.6 nM	0-8 μM	3 min	-	Fluorescent and Photoacoustic imaging in LO2 and HepG2 cells, tumor bearing mice
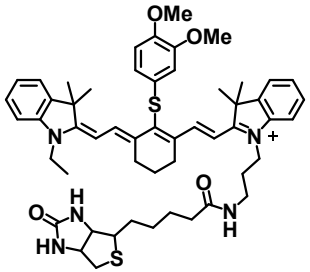 [4]	Cys	645/760	0.07 μM	3-100 μM	30 min	-	Fluorescent and Photoacoustic imaging in cells, tumor bearing mice
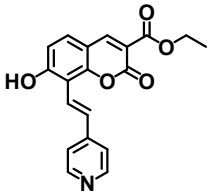 [5]	GSH	410/510 to 350/460	245 nM	0-6 mM	-	-	Imaging of GSH dynamics in the nucleoli in the cell cycle process

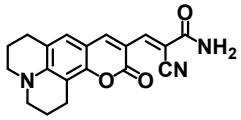 [6]	GSH	530/587 to 420/505	-	-	10 s	-	Quantitative and real-time imaging in living cells
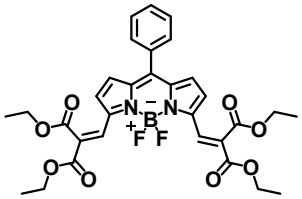 [7]	GSH	594/613 to 527/544	-	-	-	-	Real-time quantitative imaging of GSH fluctuation in living cells
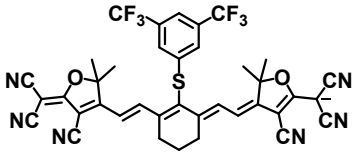 [8]	GSH	892/928	80 nM	0-20 μM	60 min	16-fold	NIR-II imaging in living cells and tumor bearing mice
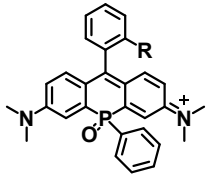 [9]	GSH	710/736	-	-	-	-	Ratiometric quantitative and real-time imaging in living cells and mice
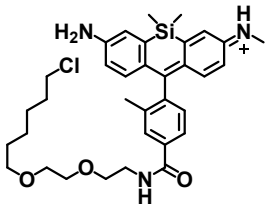 [10]	GSH	-	-	-	-	-	Quantification of redox potential and GSH concentration
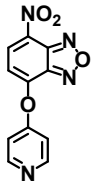 [11]	Hcy	488/550	0.084 ppm	-	5 min	-	Monitoring Hcy level in plasma from the GBM-xenograft mouse model

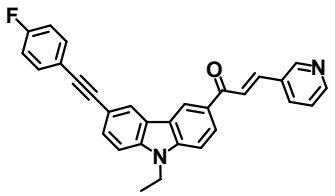 [12]	Hcy	345/456	18 nM	0-10 μM	60 min	-	Monitoring Hcy level in serum, living cells, and atherosclerosis model mice
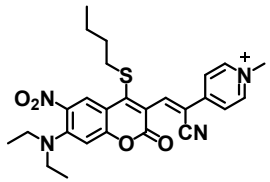 [13]	Hcy	568/654	3.7 nM	0-8 μM	30 min	357-fold	Monitoring Hcy in type 2 diabetes mellitus and Alzheimer's disease
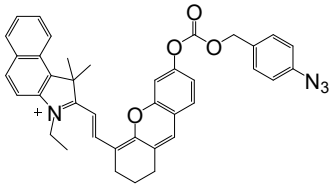 [14]	H_2S	716/736	20 nM	0-40 μM	30 min	-	Image H_2S in mitochondria of MCF-7 cells and living nude mice
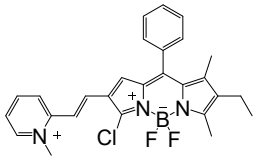 [15]	H_2S	644/718	60 nM	0-30 μM	1200 s	28-fold	Visualize and differentiate of cancers
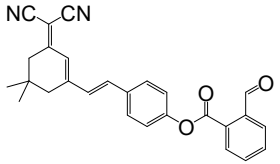 [16]	H_2S	500/650	39.1 nM	0-40 μM	12 min	-	Visualize exogenous/endogenous H2S in HeLa cells and zebrafish

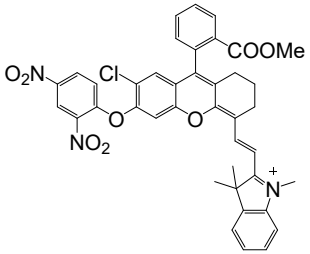 [17]	H_2S	698/729	0.51 μM	0-100 μM	-	13.5-fold	Monitor of hepatic H_2S levels in the pathological progression of nonalcoholic fatty liver disease
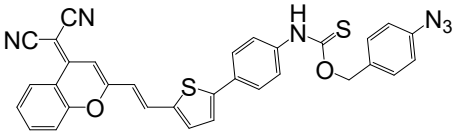 [18]	H_2S	450/670	1.3 nM	1-80 μM	40 min	25-fold	H_2S triggered and H_2S releasing fluorescent probe did not interfere with the progression of ferroptosis
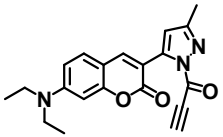 [19]	Cys Hcy	425/495	49 nM 51 nM	0-10 μM	3 min		Imaging in cells and mouse liver slice
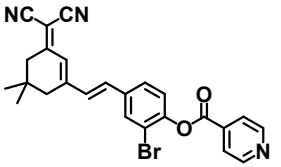 [20]	Cys Hcy GSH	537/675	68 nM 69 nM 52 nM	0-60 μM	150 s 250 s 140s	36-fold	Revealing the negative relationship between the level of thiols and the occurrence of epilepsy
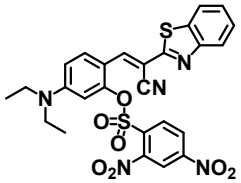 [21]	Cys Hcy GSH	458/528	78.8 nM 90.5 nM 86.4 nM	0-4.5 μM 0-4.5 μM 0-5 μM	60 s	180-fold	Imaging in cells and mouse tissues

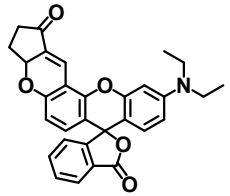 [22]	Cys Hcy GSH	494/557	70 nM 49 nM 62 nM	0-10 μM	10 s	82-fold	Imaging in HeLa cells and labeling sulfhydryl-containing proteins
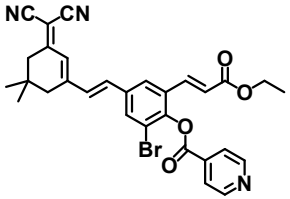 [23]	Cys Hcy GSH	541/713	27 nM 74 nM 55 nM	0-20 μM	9 min 27 min 20 min	65-fold 49-fold 57-fold	Imaging changes of biothiols in vivo in the brains of mice during CIRI
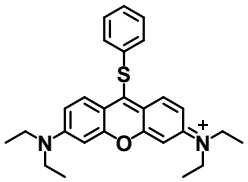 [24]	Cys Hcy	580/620 to 445/540	22 nM 23 nM	2-8 μM 4-12 μM	5 min 10 min	163-fold 125-fold	Visualizing mitochondrial biothiols in living cells and Daphnia magna model
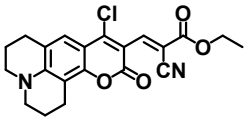 [25]	Cys Hcy GSH	397/503 375/467 500/568	0.2 nM 0.7 nM 1 nM	0-30 μM 0-30 μM 0-10 μM	 15 min	740-fold 457-fold 115-fold	Visualizing endogenous Hcy, Cys, GSH, and their transformation in living cells
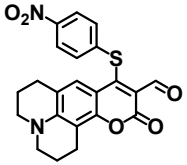 [26]	Cys Hcy GSH	396/495 396/495 505/565	106 nM 82 nM 57 nM	0-30 μM 0-30 μM 0-15 μM	25 min 25 min 20 min	119-fold 130-fold 288-fold	Discrimination of different biothiols in cells and zebra fish

References for Table S1

[1] Y. Zhang, X. Wang, X. Bai, P. Li, D. Su, W. Zhang, W. Zhang, B. Tang, Highly Specific Cys Fluorescence Probe for Living Mouse Brain Imaging via Evading Reaction with Other Biothiols, Anal. Chem. 91 (2019) 8591–8594. https://doi.org/10.1021/acs.analchem.9b01878

[2] E. Karakuş, M. Sayar, S. Dartar, B.U. Kaya, M. Emrullahoğlu, Fluorescein propiolate: a propiolate-decorated fluorescent probe with remarkable selectivity towards cysteine, Chem. Commun. 55 (2019) 4937–4940. https://doi.org/10.1039/C9CC01774G

[3] Z. Chen, B. Wang, Y. Liang, L. Shi, X. Cen, L. Zheng, E. Liang, L. Huang, K. Cheng, Near-Infrared Fluorescent and Photoacoustic Dual-Mode Probe for Highly

Sensitive and Selective Imaging of Cysteine In Vivo, Anal. Chem. 94 (2022) 10737–10744. https://doi.org/10.1021/acs.analchem.2c01372

[4] Q.-S. Gu, Z.-C. Yang, J.-J. Chao, L. Li, G.-J. Mao, F. Xu, C.-Y. Li, Tumor-Targeting Probe for Dual-Modal Imaging of Cysteine In Vivo, Anal. Chem. 95 (2023) 12478–12486. https://doi.org/10.1021/acs.analchem.3c02134

[5] S. Khatun, S. Yang, Y.Q. Zhao, Y. Lu, A. Podder, Y. Zhou, S. Bhuniya, Highly Chemoselective Self-Calibrated Fluorescent Probe Monitors Glutathione Dynamics in Nucleolus in Live Cells, Anal. Chem. 92 (2020) 10989–10995. https://doi.org/10.1021/acs.analchem.9b05175

[6] M. Tian, X.-Y. Liu, H. He, X.-Z. Ma, LC. iang, Y. Liu, F.-L. Jiang, Real-Time Imaging of Intracellular Glutathione Levels Based on a Ratiometric Fluorescent Probe with Extremely Fast Response, Anal. Chem. 2020, 92, 10068–10075. https://doi.org/10.1021/acs.analchem.0c01881

[7] H. Liu, W. Song, S. Zhang, K.S. Chan, Z. Guo, Z. Shen, A ratiometric fluorescent probe for real-time monitoring of intracellular glutathione fluctuations in response to cisplatin, Chem. Sci. 11 (2020) 8495–8501. https://doi.org/10.1039/D0SC02889D

[8] Y. Pan, S. Lei, J. Zhang, J. Qu, P. Huang, J. Lin, Activatable NIR-II Fluorescence Probe for Highly Sensitive and Selective Visualization of Glutathione In Vivo, Anal. Chem. 93 (2021) 17103–17109. https://doi.org/10.1021/acs.analchem.1c04504

[9] N. Li, T. Wang, N. Wang, M. Fan, X. Cui, A Substituted-Rhodamine-Based Reversible Fluorescent Probe for In Vivo Quantification of Glutathione, Angew. Chem. Int. Ed. 62 (2022) e202217326. https://doi.org/10.1002/anie.202217326

[10] S. Emmert, G. Quargnali, S. Thallmair, P. Rivera-Fuentes, A locally activatable sensor for robust quantification of organellar glutathione, Nat. Chem. 15 (2023) 1415–1421. https://doi.org/10.1038/s41557-023-01249-3

[11] Y. Kim, J.M. An, J. Kim, T. Chowdhury, H.J. Yu, K.-M. Kim, H. Kang, C.-K. Park, J. F. Joung, S. Park, D. Kim, Pyridine-NBD: A homocysteine-selective fluorescent probe for glioblastoma (GBM) diagnosis based on a blood test, Anal. Chim. Acta 1202 (2022) 339678. https://doi.org/10.1016/j.aca.2022.339678

[12] F. Wei, Y. Ding, J. Ou, CX. hen, L. Li, Q. Zhou, Q. Chen, Q. Wang, Y. Feng, X. Meng, Accurate Detection of Hcy in Human Serum and Two-Photon Visualization of Atherosclerosis Using a Highly Specific Fluorescent Probe, Anal. Chem. 95 (2023) 9173–9181. https://doi.org/10.1021/acs.analchem.2c05441

[13] T. Zhou, Y. Yang, K. Zhou, M. Jin, M. Han, W. Li, C. Yin, Efficiently mitochondrial targeting fluorescent imaging of H2S in vivo based on a conjugate-lengthened cyanine NIR fluorescent probe, Actuat. B-Chem. 301 (2019) 127116. https://doi.org/10.1016/j.snb.2019.127116.

[14] R. Wang, X. Gu, Q. Li, J. Gao, B. Shi, G. Xu, T. Zhu, H. Tian, C. Zhao, Aggregation Enhanced Responsiveness of Rationally Designed Probes to Hydrogen Sulfide for Targeted Cancer Imaging, J. Am. Chem. Soc. 142 (2020) 15084−15090. https://dx.doi.org/10.1021/jacs.0c06533.

[15] W. Shu, S. Zang, C. Wang, M. Gao, J. Jing, X. Zhang, An Endoplasmic Reticulum-Targeted Ratiometric Fluorescent Probe for the Sensing of Hydrogen Sulfide in Living Cells and Zebrafish, Anal. Chem. 92 (2020) 9982−9988. https://dx.doi.org/10.1021/acs.analchem.0c01623.

[16] W. Li, Y. Shen, X. Gong, X.-B. Zhang, L. Yuan, Highly Selective Fluorescent Probe Design for Visualizing Hepatic Hydrogen Sulfide in the Pathological Progression of Nonalcoholic Fatty Liver, Anal. Chem. 93 (2021) 16673−16682. https://doi.org/10.1021/acs.analchem.1c04246.

[17] T. Liang, T. Qiang, L. Ren, F. Cheng, B. Wang, M. Li, W. Hu, T.D. James, Near-infrared fluorescent probe for hydrogen sulfide: high-fidelity ferroptosis

evaluation in vivo during stroke, Chem. Sci. 13 (2022) 2992−3001. https://doi.org/10.1039/D1SC05930K.

[18] G. Yin, Y. Gan, H. Jiang, T. Yu, M. Liu, Y. Zhang, H. Li, P. Yin, S. Yao, General Strategy for Specific Fluorescence Imaging of Homocysteine in Living Cells and In Vivo, Anal. Chem. 95 (2023) 8932–8938. https://doi.org/10.1021/acs.analchem.3c00799

[19] T. Cheng, W. Huang, D. Gao, Z. Yang, C. Zhang, H. Zhang, J. Zhang, H. Li, X.-F. Yang, Michael Addition/S,N-Intramolecular Rearrangement Sequence Enables Selective Fluorescence Detection of Cysteine and Homocysteine, Anal. Chem. 91 (2019) 10894–10900. https://doi.org/10.1021/acs.analchem.9b02814

[20] Y. Yang, Y. Zhang, M. Ma, H. Liu, K. Ge, C. Zhang, M. Jin, D. Liu, WS. ang, C. Yin, J. Zhang, Synergistic Modulation by Halogens and Pyridine Crossing the Blood-Brain Barrier for InSitu Visualization of Thiol Flux in the Epileptic Brain, Anal. Chem. 94 (2022) 14443–14452. https://doi.org/10.1021/acs.analchem.2c03390

[21] Y. Zhang, N. Zhang, S. Wang, Q. Zan, X. Wang, Q. Yang, X. Yu, C. Dong, L. Fan, A lipid droplet-targetable and biothiol-sensitive fluorescent probe for the diagnosis of cancer cells/tissues, Analyst 147 (2022) 1695–1701. https://doi.org/10.1039/D2AN00030J

[22] S. Zheng, J. Peng, L. Jiang, H. Gu, F. Wang, C. Wang, S. Lu, C. Chen, A rhodol-derived probe for intracellular biothiols imaging and rapid labelling of sulfhydryl-containing proteins, Sens. Actuators B: Chem. 367 (2022) 132148. https://doi.org/10.1016/j.snb.2022.132148

[23] Y. Yang, M. Ma, L. Shen, J. An, E. Kim, H. Liu, M. Jin, S. Wang, J. Zhang, J. S. Kim, C. Yin, A Fluorescent Probe for Investigating the Role of Biothiols in Signaling Pathways Associated with Cerebral Ischemia-Reperfusion Injury, Angew. Chem.Int. Ed. 62 (2023) e202310408. https://doi.org/10.1002/anie.202310408

[24] M. Yang, J. Fan, W. Sun, J. Du, X. Peng, Mitochondria-Anchored Colorimetric and Ratiometric Fluorescent Chemosensor for Visualizing Cysteine/Homocysteine in Living Cells and Daphnia magna Model, Anal. Chem. 91 (2019) 12531–12537. https://doi.org/10.1021/acs.analchem.9b03386

[25] G. Yin, T. Niu, T. Yu, Y. Gan, X. Sun, P. Yin, H. Chen, Y. Zhang, H. Li, S. Yao, Simultaneous Visualization of Endogenous Homocysteine, Cysteine, Glutathione, and their Transformation through Different Fluorescence Channels, Angew. Chem.Int. Ed. 58 (2019) 4557–4561. https://doi.org/10.1002/anie.201813935

[26] X.-B. Wang, H.-J. Li, C. Liu, Y.-X. Hu, M.-C. Li, Y.-C. Wu, Simple Turn-On Fluorescent Sensor for Discriminating Cys/Hcy and GSH from Different Fluorescent Signals, Anal. Chem. 93 (2021) 2244–2253. https://doi.org/10.1021/acs.analchem.0c04100

Table S2. Comparison of reported nitro-1,2,3-benzoxadiazole modified probes and the present probe NBD-2FDCI.

Probe	Analyte	$\lambda_{ex}/\lambda_{em}$ (nm)	LOD	Linear range	Response time	Enhance-ment	Applications
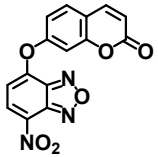 [1]	Cys	330/480	0.024 μM	0-10 μM	-	86-fold	Imaging in HeLa cells
		460/580	0.020 μM	0-80 μM		508-fold	
	Hcy	330/480	0.142 μM	0-30 μM	-	90-fold	
		460/580	0.010 μM	0-25 μM		580-fold	
	GSH	330/480	0.018 μM	0-6 μM	-	92-fold	
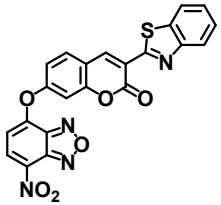 [2]	H_2S	450/490	0.12 μM	0-20 μM	2 min	125-fold	Fast imaging of H_2S in living cells and different fresh tissues
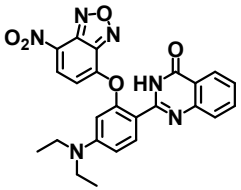 [3]	Cys	475/525	11.4 nM	0-10 μM	15 min	-	Distinguishing between tumor cells and normal cells, high toxicity to tumor cells
	Hcy	475/525	16.8 nM	0-10 μM	30 min	-	
	GSH	425/545	145.4 nM	0-10 μM	30 min	-	
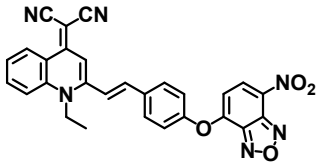 [4]	Cys	460/560	0.06 μM	0-100 μM	15 min	-	Imaging in HeLa cells
	Hcy	460/560	0.084 μM	0-50 μM	15 min	-	

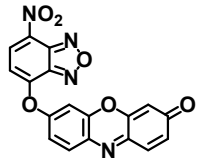 [5]	Cys	470/540		3.1-90 μM	5 min	86-fold	Simultaneous determination of Cys and GSH in human plasma
		470/585	0.13 μM	1-40 μM		41-fold	
	GSH	470/585	0.07 μM	1-18 μM	5 min	43-fold	
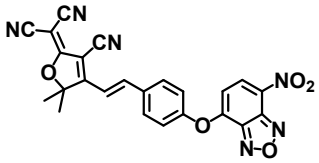 [6]	Cys	470/547	15 nM	0-40 μM	10 min	-	Imaging intracellular biothiols in living cells and Daphnia magna
		570/610		0-25 μM			
	Hcy	470/547	34 nM	0-60 μM	10 min		
		570/610		0-60 μM			
	GSH	570/610	30 nM	0-20 μM	10 min		
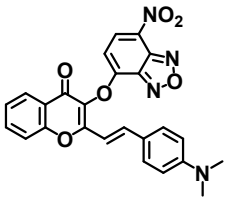 [7]	Cys	470/547	2.1 μM	0-500 μM	60 min	-	Imaging in HeLa cells
		570/610					
	Hcy	470/547	2.7 μM	0-500 μM	60 min		
		570/610					
	GSH	570/621	6.4 μM	0-600 μM	60 min		
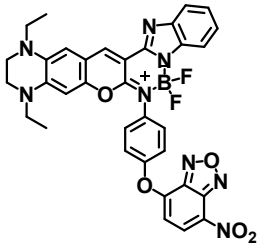 [8]	Cys	490/565	95.6 nM	20-160 μM	7 min	-	Distinguishing Cys/Hcy from GSH in real biological systems
		490/630					
	Hcy	490/565	24.7 nM	0-140 μM	7 min		
		490/630					
	GSH	490/630	39.3 nM	20-160 μM	7 min		
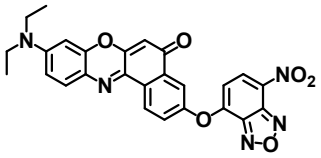 [9]	Cys	470/543	0.13 μM	0-70 μM	180 s	-	Imaging in MCF-7 cells
		470/636					
	H_2S	565/636	0.05 μM	0-75 μM	30 s		

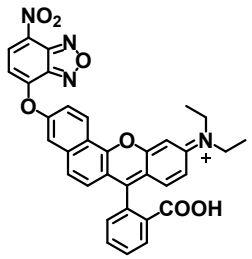 [10]	Cys	435/543	52 nM	0-15 μM	20 min	-	Imaging in living cells and zebrafish
		435/643					
	Hcy	435/543	77 nM	0-15 μM	20 min		
		435/643					
	GSH	435/643	65 nM	0-15 μM	20 min		
	H_2S	435/643	62 nM	0-15 μM	20 min		
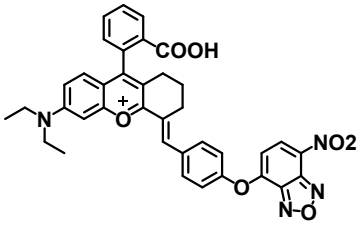 [11]	Cys	481/556	0.248 μM	20-120 μM	3 min	-	Imaging in HeLa cells
		570/668					
	Hcy	481/556	0.251 μM	0-200 μM	8 min		
		570/668					
	GSH	395/499	0.31 μM	0-60 μM	30 min		
		570/668	0.28 μM	0-70 μM			
	H_2S	570/668	1.5 μM	0-300 μM	25 min		
	SO_2	395/499	0.365 μM	20-70 μM	27 min		
		570/668					
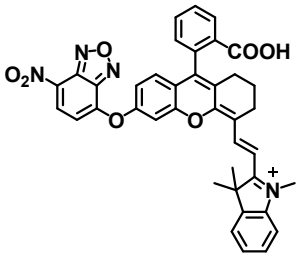 [12]	Cys	463/544	21 nM	2-150 μM	7 min	-	Distinguishing Cys/Hcy in cellular context by dual-color fluorescence imaging
		650/707					
	Hcy	463/544	37 nM	2-200 μM	20 min		
		650/707					
	GSH	650/707	28 nM	2-100 μM	10 min		
	H_2S	650/707	15 nM	2-70 μM	10 min		

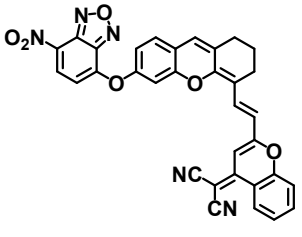 [13]	H_2S	613/744	26 nM	0-25 μM	3 min	40-fold	Imaging exogenous and endogenous H_2S in living cells and rapid imaging of H_2S in living mice
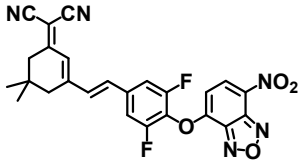 This Work	Cys	480/550	1.1 μM	5-200 μM	45 min	58.3-fold	Endogenous and exogenous biothiols and H_2S imaging, and measurement in urine samples of bladder cancer (BC) patients
		480/661	1.5 μM	5-200 μM		56.3-fold	
	Hcy	480/550	0.98 μM	5-200 μM		85.8-fold	
		480/661	1.9 μM	5-200 μM		58.7-fold	
	GSH	480/661	4.2 μM	10-500 μM		67.1-fold	
	H_2S	480/661	0.35 μM	1-50 μM		64.1-fold	

References for Table S2

[1] L. Zhai, Z. Shi, Y. Tu, S. Pu, A dual emission fluorescent probe enables simultaneous detection and discrimination of Cys/Hcy and GSH and its application in cell imaging, Dyes Pigments 165 (2019) 164−171. https://doi.org/10.1016/j.dyepig.2019.02.010

[2] Q. Chen, J. Yang, Y. Li, J. Zheng, R. Yang, Sensitive and rapid detection of endogenous hydrogen sulfide distributing in different mouse viscera via a two-photon fluorescent probe, Anal. Chim. Acta 896 (2015) 128−136. http://dx.doi.org/10.1016/j.aca.2015.05.040

[3] Y. Zhang, C. Liu, W. Sun, Z. Yu, M. Su, X. Rong, X. Wang, K. Wang, X. Li, H. Zhu, M. Yu, W. Sheng, B. Zhu, Concise Biothiol-Activatable HPQ-NBD Conjugate as a Targeted Theranostic Probe for Tumor Cells, Anal. Chem. 94 (2022) 7140−7147. https://doi.org/10.1021/acs.analchem.2c01459

[4] W. Wang, M. Ji, J. Chen, P. Wang, A novel turn-on type AIE fluorescent probe for highly selective detection of cysteine/homocysteine and its application in living cells, Talanta 239 (2022) 123091. https://doi.org/10.1016/j.talanta.2021.123091

[5] X. Gao, X. Li, L. Li, J. Zhou, H. Ma, A simple fluorescent off-on probe for the discrimination of cysteine from glutathione, Chem. Commun. 51 (2015) 9388−9390. https://doi.org/10.1039/C5CC02788H

[6] M. Yang, J. Fan, W. Sun, J. Du, S. Long, X. Peng, Simultaneous visualization of cysteine/homocysteine and glutathione in living cells and Daphnia magna via dual-signaling fluorescent chemosensor, Dyes Pigments 168 (2019) 189−196. https://doi.org/10.1016/j.dyepig.2019.04.056

[7] W. Chen, H. Luo, X. Liu, J.W. Foley, X. Song, Broadly Applicable Strategy for the Fluorescence Based Detection and Differentiation of Glutathione and Cysteine/Homocysteine: Demonstration in Vitro and in Vivo, Anal. Chem. 88 (2016) 3638−3646. https://doi.org/10.1021/acs.analchem.5b04333

[8] X. Ren, Y. Zhang, F. Zhang, H. Zhong, J. Wang, X. Liu, Z. Yang , X. Song, Red-emitting fluorescent probe for discrimination of Cys/Hcy and GSH with a large Stokes shift under a single-wavelength excitation, Anal. Chim. Acta 1097 (2020) 245−253. https://doi.org/10.1016/j.aca.2019.11.030

[9] H. Niu, B. Ni, K. Chen, X. Yang, W. Cao, Y. Ye, Y. Zhao, A long-wavelength-emitting fluorescent probe for simultaneous discrimination of H2S/Cys/GSH and its bio-imaging applications, Talanta 196 (2019) 145−152. https://doi.org/10.1016/j.talanta.2018.12.031

[10] H. Zhu, C. Liu, R. Yuan, R. Wang, H. Zhang, Z. Li, P. Jia, B. Zhu, W. Sheng, A simple highly specific fluorescent probe for simultaneous discrimination of cysteine/homocysteine and glutathione/hydrogen sulfide in living cells and zebrafish using two separated fluorescence channels under single wavelength excitation, Analyst 144 (2019) 4258−4265. https://doi.org/10.1039/C9AN00818G

[11] Y. Zhang, L. Wen, W. Zhang, Y. Yue, J. Chao, F. Huo, C. Yin, Sulphide activity-dependent multicolor emission dye and its applications in in vivo imaging, Analyst 146 (2021) 5517−5527. https://doi.org/10.1039/D1AN01345A

[12] X. Yang, L. He, K. Xu, W. Lin, A fluorescent dyad with large emission shift for discrimination of cysteine/homocysteine from glutathione and hydrogen sulfide and the application of bioimaging, Anal. Chim. Acta 981 (2017) 86−93. http://dx.doi.org/10.1016/j.aca.2017.05.016

[13] S. Gong, E. Zhou, J. Hong, G. Feng, Nitrobenzoxadiazole Ether-Based Near-Infrared Fluorescent Probe with Unexpected High Selectivity for H2S Imaging in Living Cells and Mice, Anal. Chem. 91 (2019) 13136−13142.

3. Supplementary NMR and MS spectra

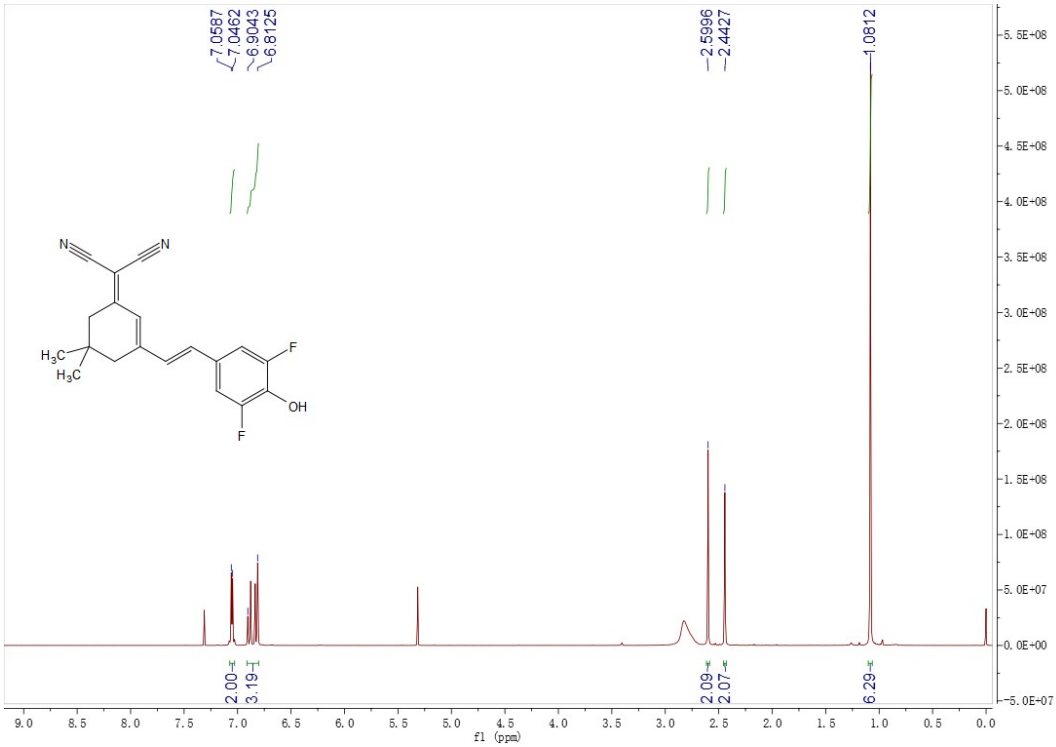

Figure S22. ^{1}H NMR Spectrum of **2FDCI**.

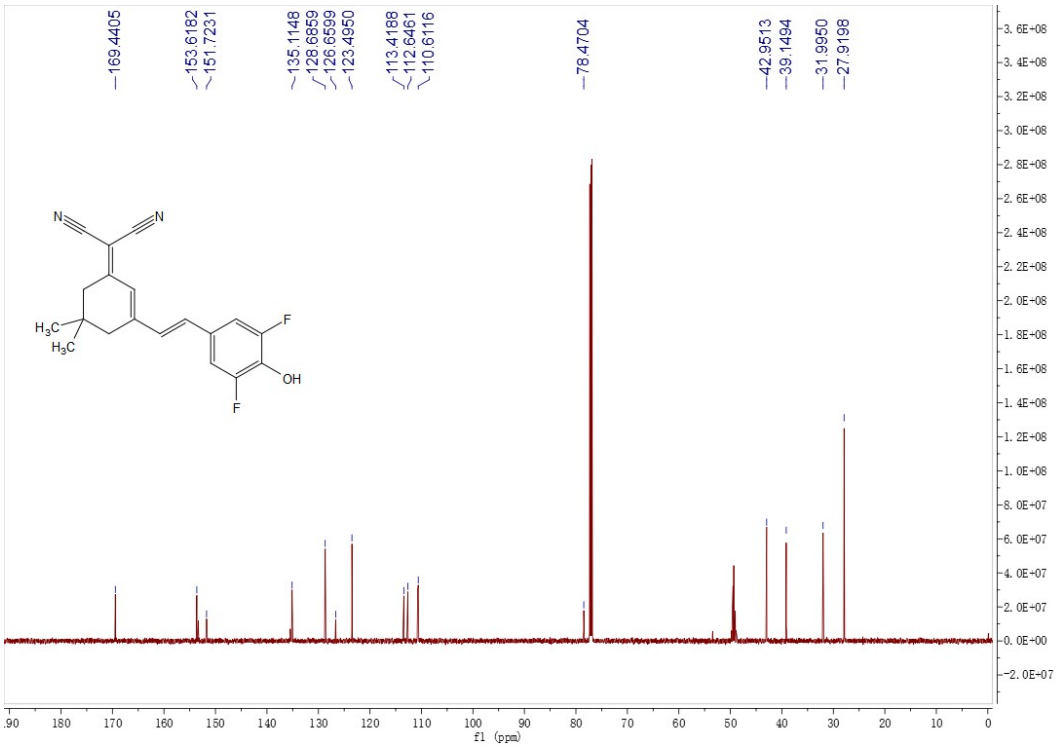

Figure S23. ^{13}C NMR Spectrum of **2FDCI**.

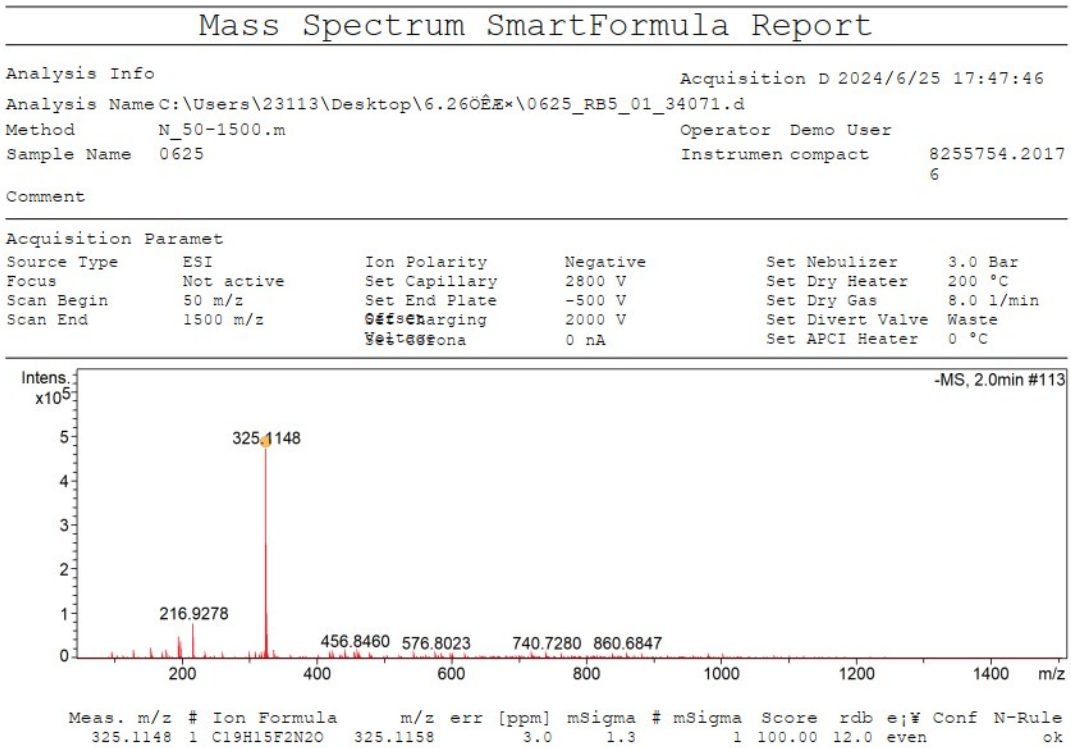

Figure S24. Mass Spectrum of **2FDCI**.

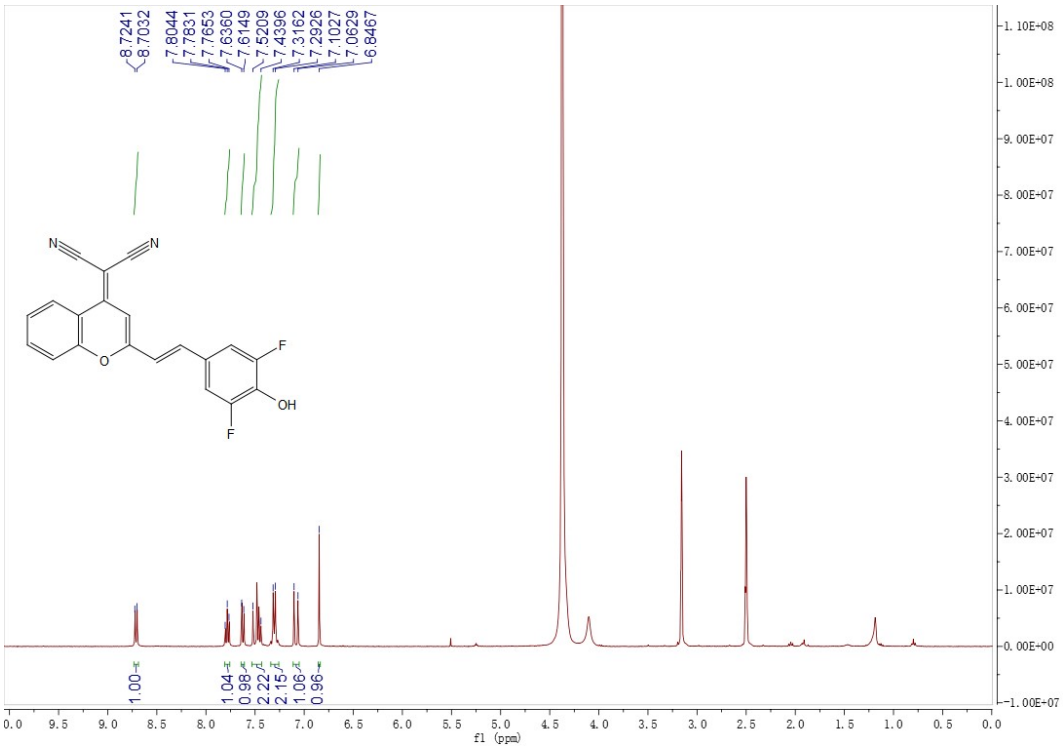

Figure S25. ^{1}H NMR Spectrum of **2FDCM**.

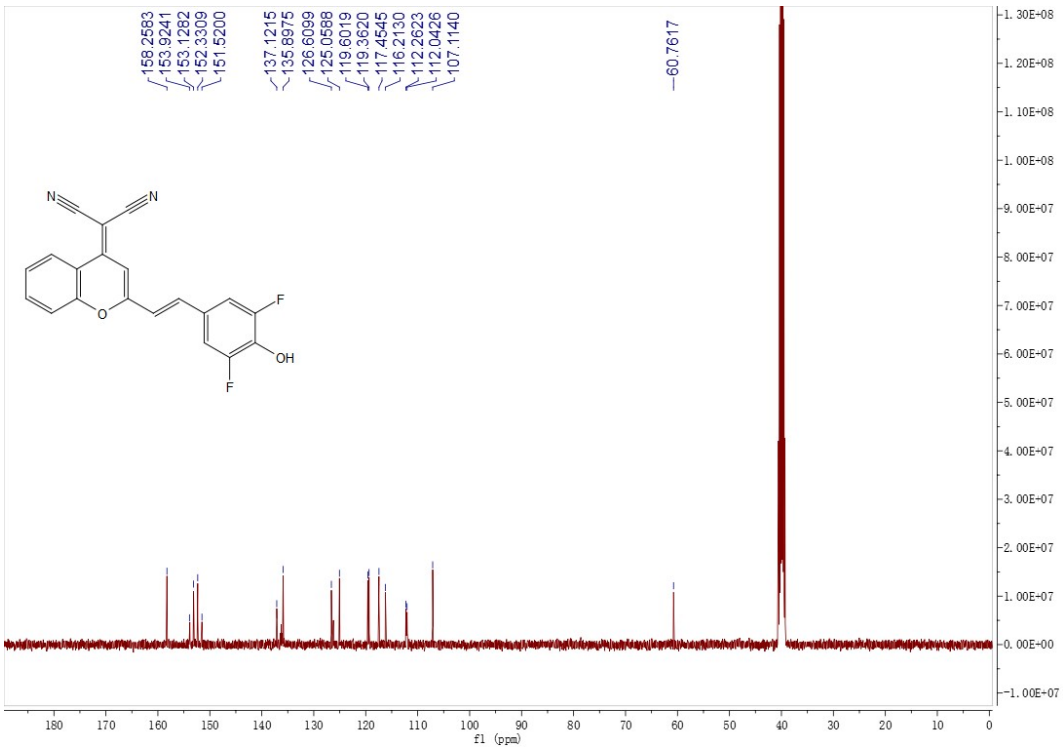

Figure S26. ^{13}C NMR Spectrum of **2FDCM**.

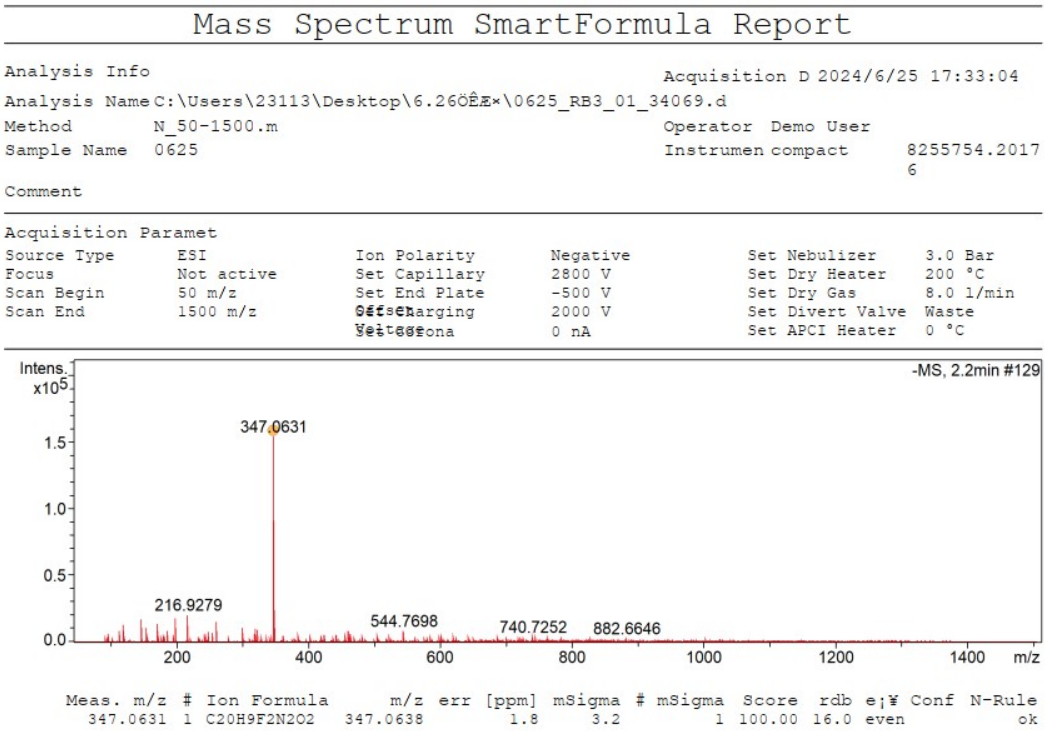

Mass Spectrum SmartFormula Report

Analysis Info — Acquisition D 2024/6/25 17:33:04

Analysis Name C:\Users\23113\Desktop\6.26ÖÊÆ×\0625_RB3_01_34069.d

Method N_50-1500.m — Operator Demo User

Sample Name 0625 — Instrumen compact 8255754.2017 6

Comment

Acquisition Paramet

Source Type	ESI	Ion Polarity	Negative	Set Nebulizer	3.0 Bar
Focus	Not active	Set Capillary	2800 V	Set Dry Heater	200 °C
Scan Begin	50 m/z	Set End Plate	-500 V	Set Dry Gas	8.0 l/min
Scan End	1500 m/z	Set Charging	2000 V	Set Divert Valve	Waste
		Set Corona	0 nA	Set APCI Heater	0 °C

Meas. m/z	#	Ion Formula	m/z	err [ppm]	mSigma	# mSigma	Score	rdb	e¡¥	Conf	N-Rule
347.0631	1	C20H9F2N2O2	347.0638	1.8	3.2	1	100.00	16.0	even		ok

Figure S27. Mass Spectrum of **2FDCM**.

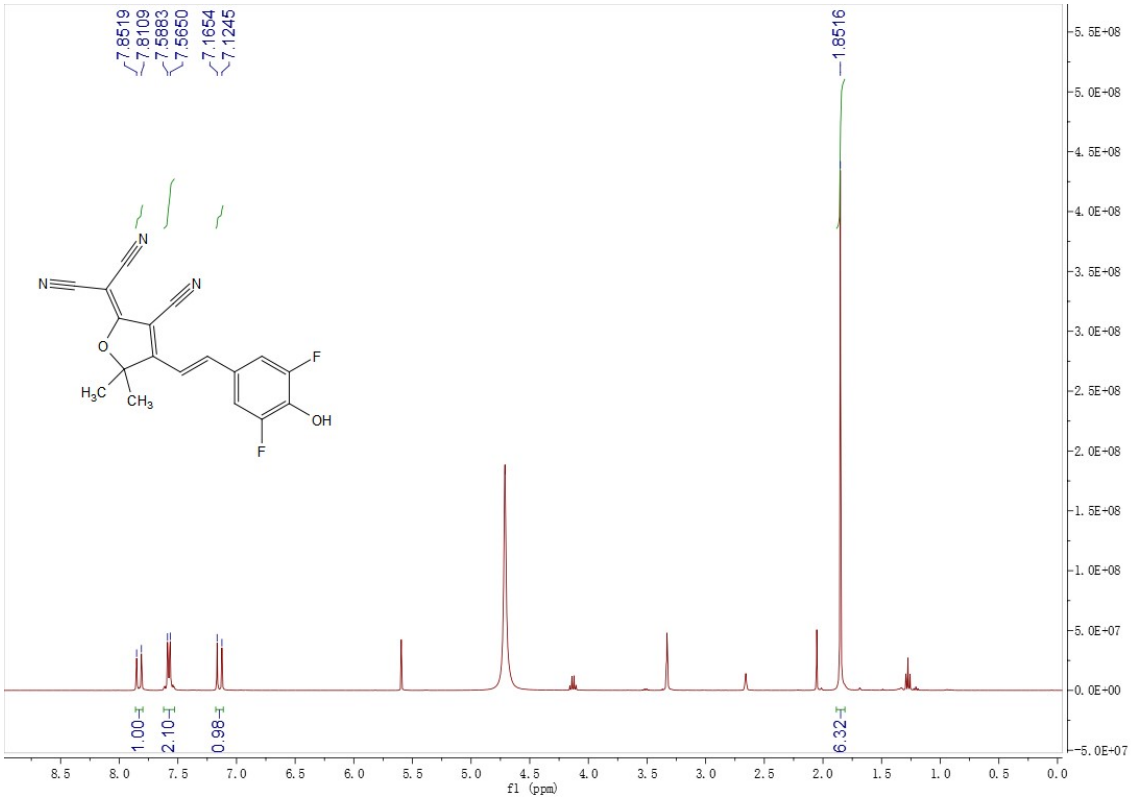

Figure S28. ^{1}H NMR Spectrum of **2FTCF**.

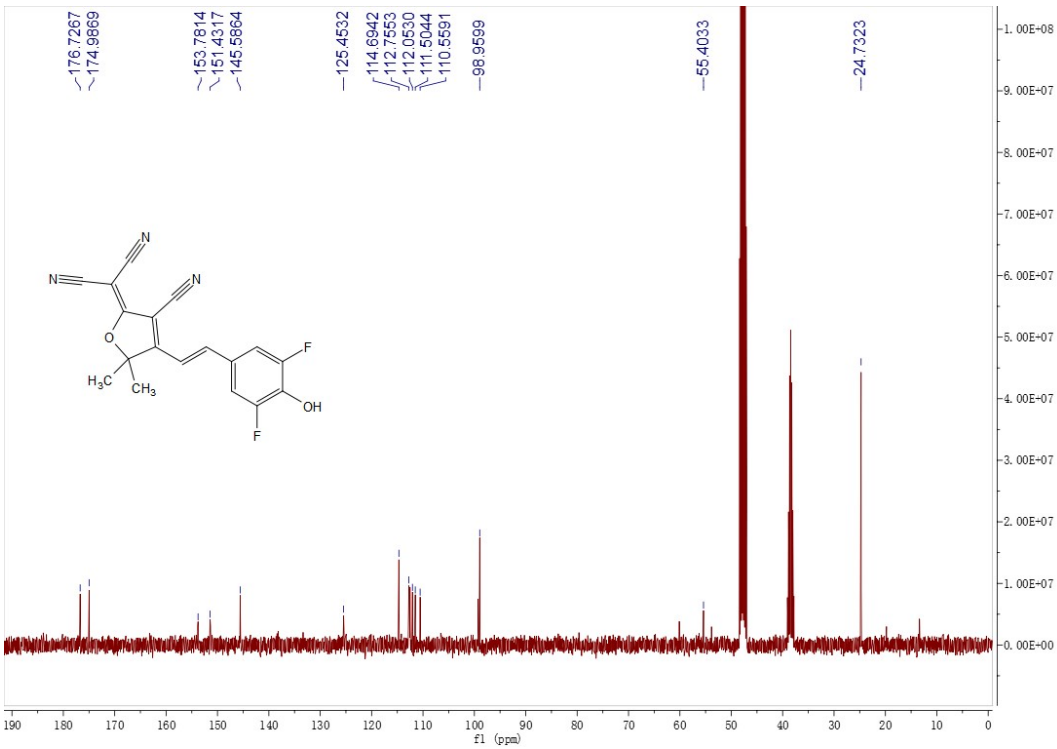

Figure S29. ^{13}C NMR Spectrum of **2FTCF**.

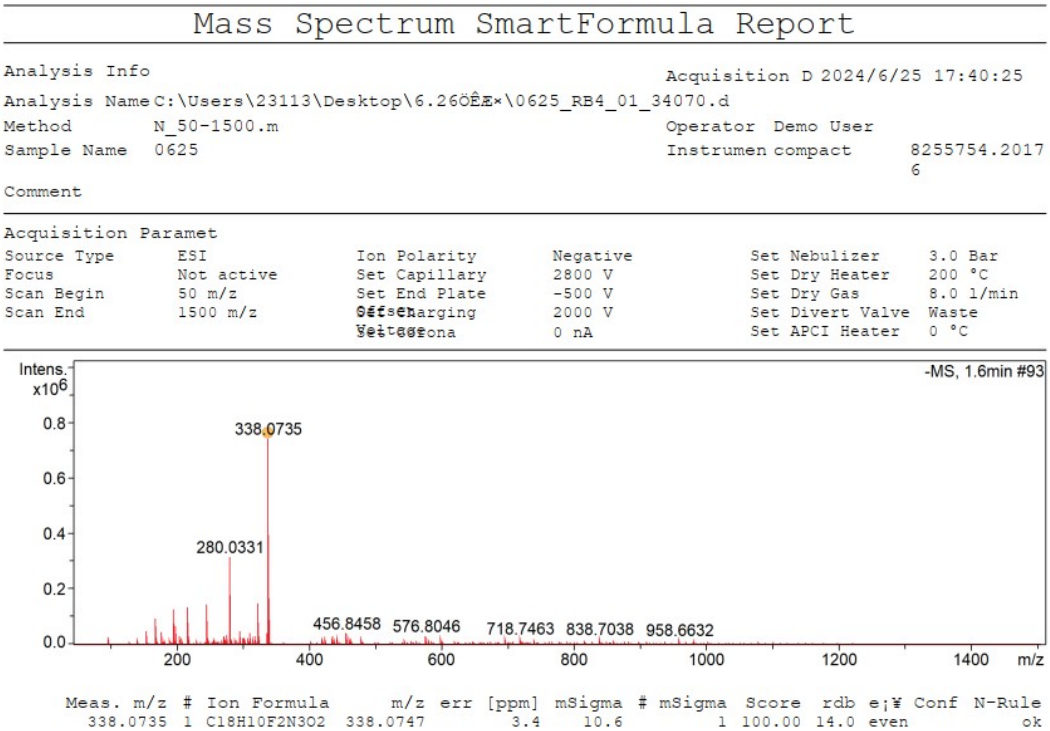

Figure S30. Mass Spectrum of **2FTCF**.

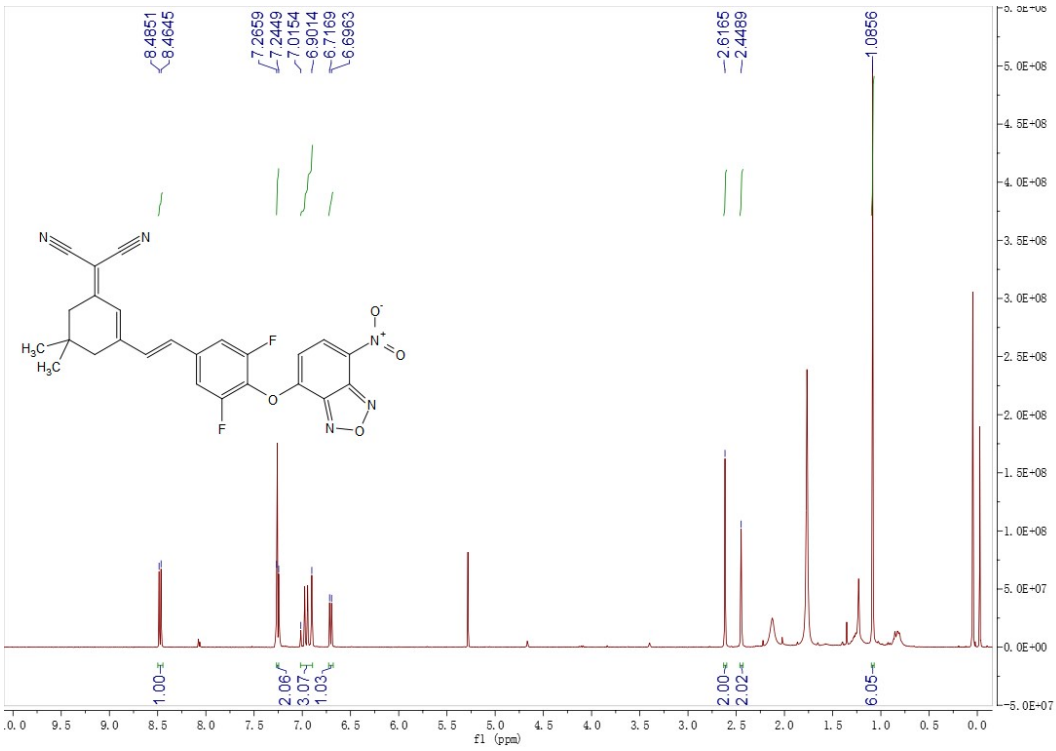

Figure S31. ^{1}H NMR Spectrum of **NBD-2FDCI**.

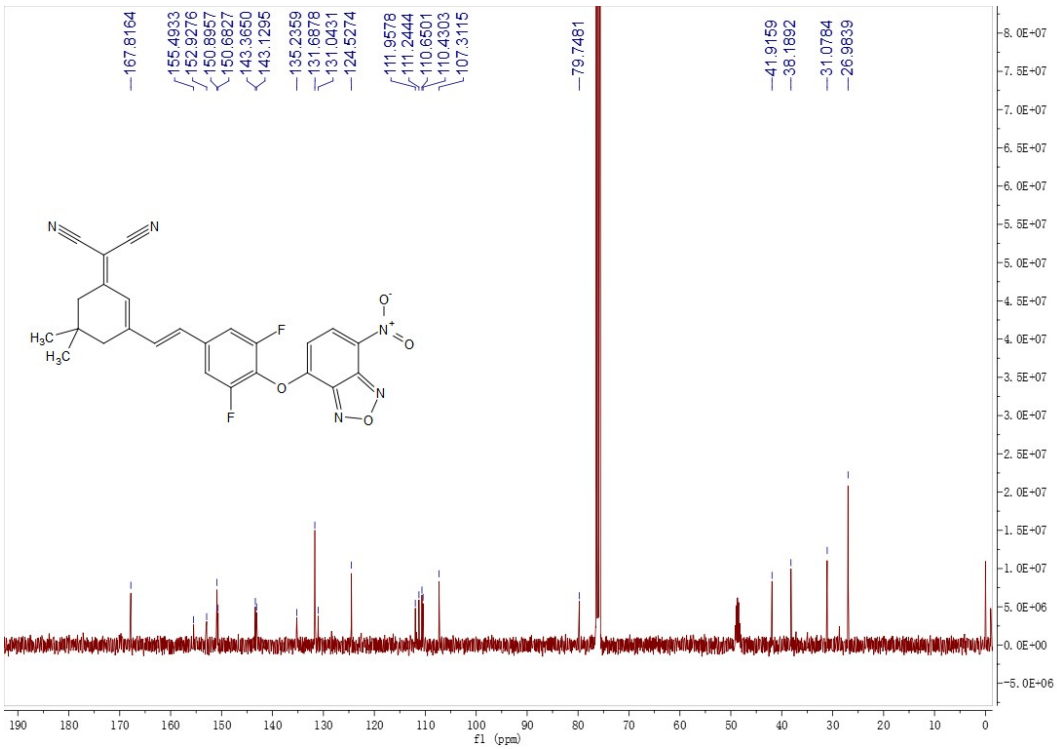

Figure S32. ^{13}C NMR Spectrum of **NBD-2FDCI**.

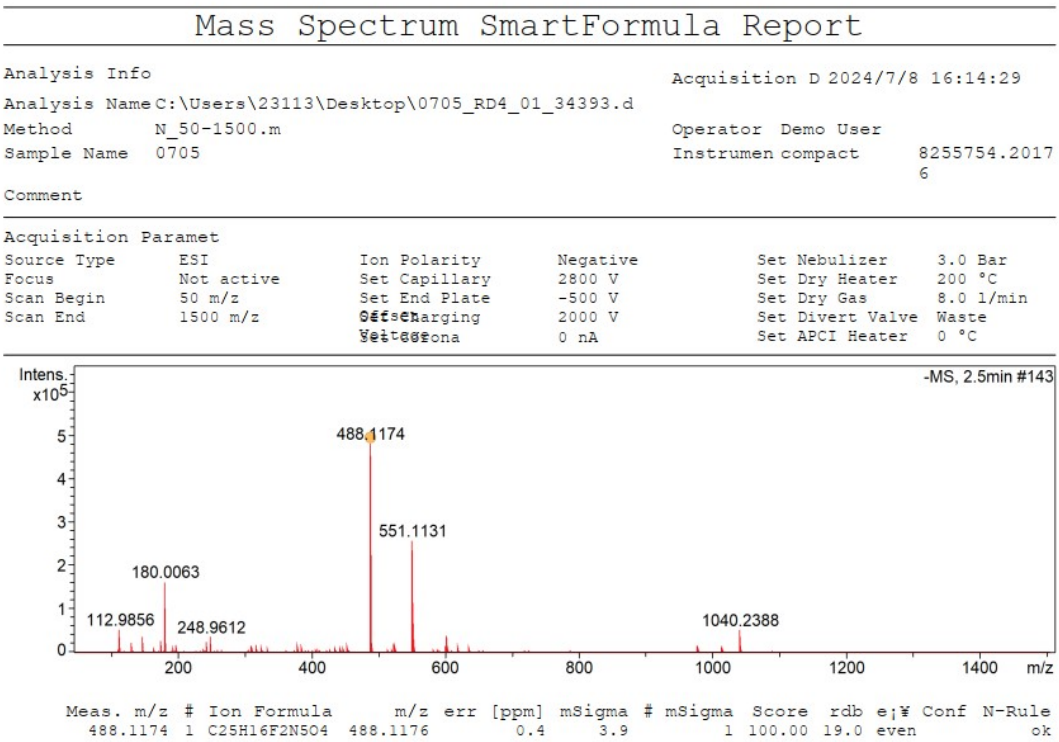

Mass Spectrum SmartFormula Report

Analysis Info

Analysis Name C:\Users\23113\Desktop\0705_RD4_01_34393.d
Method N_50-1500.m
Sample Name 0705
Comment

Acquisition D 2024/7/8 16:14:29
Operator Demo User
Instrumen compact 8255754.2017 6

Acquisition Paramet

Source Type	ESI	Ion Polarity	Negative	Set Nebulizer	3.0 Bar
Focus	Not active	Set Capillary	2800 V	Set Dry Heater	200 °C
Scan Begin	50 m/z	Set End Plate	-500 V	Set Dry Gas	8.0 l/min
Scan End	1500 m/z	Set Charging	2000 V	Set Divert Valve	Waste
		Set Corona	0 nA	Set APCI Heater	0 °C

Meas. m/z	#	Ion Formula	m/z	err [ppm]	mSigma	# mSigma	Score	rdb	e¡¥	Conf	N-Rule
488.1174	1	C25H16F2N5O4	488.1176	0.4	3.9	1	100.00	19.0	even		ok

Figure S33. Mass Spectrum of **NBD-2FDCI**.

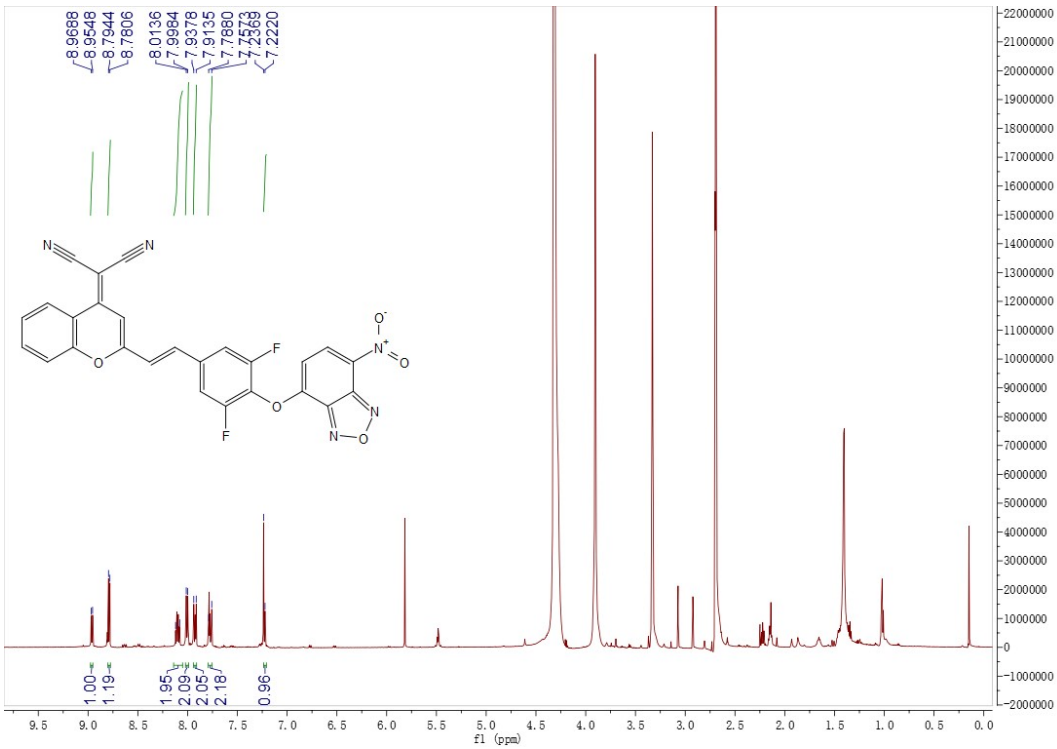

Figure S34. ^{1}H NMR Spectrum of **NBD-2FDCM**.

Mass Spectrum SmartFormula Report

Analysis Info

Analysis Name C:\Users\23113\Desktop\0705_RD5_01_34394.d
Method N_50-1500.m
Sample Name 0705
Comment

Acquisition D 2024/7/8 16:21:51
Operator Demo User
Instrumen compact 8255754.2017 6

Acquisition Paramet

Source Type	ESI	Ion Polarity	Negative	Set Nebulizer	3.0 Bar
Focus	Not active	Set Capillary	2800 V	Set Dry Heater	200 °C
Scan Begin	50 m/z	Set End Plate	-500 V	Set Dry Gas	8.0 l/min
Scan End	1500 m/z	Set Charging	2000 V	Set Divert Valve	Waste
		Set Corona	0 nA	Set APCI Heater	0 °C

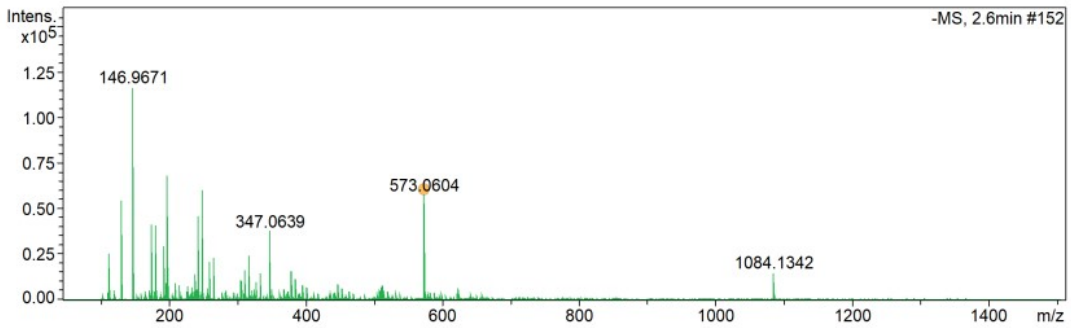

Meas. m/z	#	Ion Formula	m/z	err [ppm]	mSigma	# mSigma	Score	rdb	e¡¥	Conf	N-Rule
573.0604	1	C26H11F2N6O8	573.0612	1.3	7.9	1	100.00	23.0	even		ok

Figure S35. Mass Spectrum of **NBD-2FDCM**.

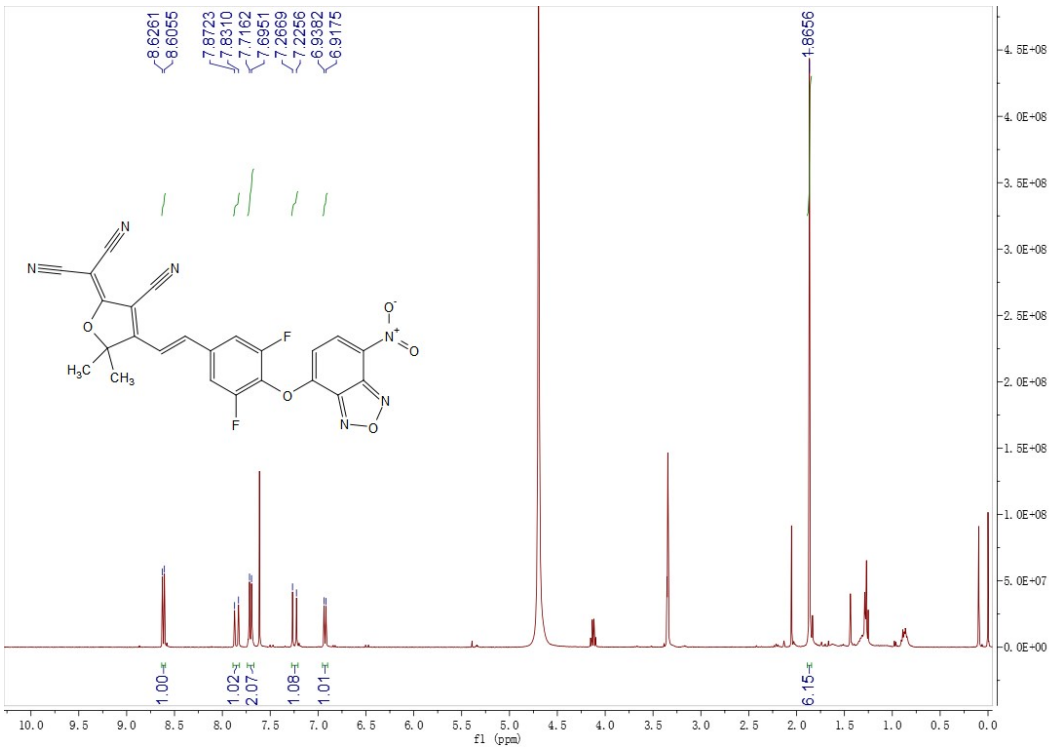

Figure S36. ^{1}H NMR Spectrum of **NBD-2FTCF**.

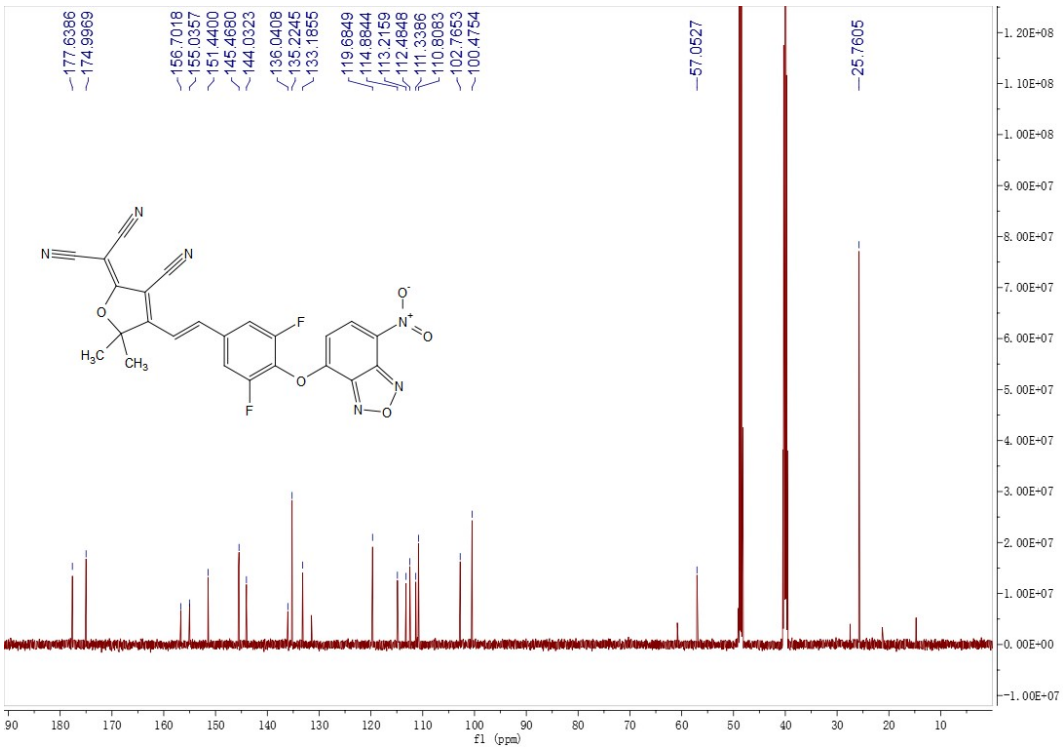

Figure S37. ^{13}C NMR Spectrum of **NBD-2FDCI**.

Mass Spectrum SmartFormula Report

Analysis Info

Acquisition D 2024/6/25 18:02:27

Analysis Name C:\Users\23113\Desktop\6.26ÖÊÆ×\0625_RB7_01_34073.d

Method N_50-1500.m

Operator Demo User

Sample Name 0625

Instrumen compact 8255754.2017 6

Comment

Acquisition Paramet

Source Type	ESI	Ion Polarity	Negative	Set Nebulizer	3.0 Bar
Focus	Not active	Set Capillary	2800 V	Set Dry Heater	200 °C
Scan Begin	50 m/z	Set End Plate	-500 V	Set Dry Gas	8.0 l/min
Scan End	1500 m/z	Set Charging	2000 V	Set Divert Valve	Waste
		Set Corona	0 nA	Set APCI Heater	0 °C

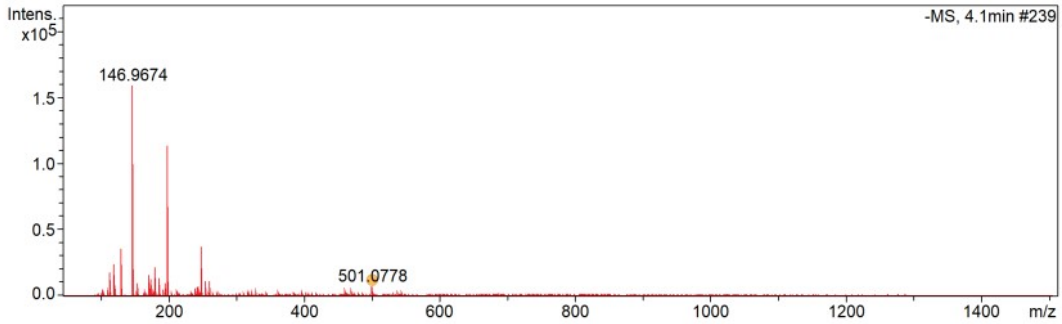

Meas. m/z	#	Ion Formula	m/z	err [ppm]	mSigma	# mSigma	Score	rdb	e¡¥	Conf	N-Rule
501.0778	1	C24H11F2N6O5	501.0764	-2.7	18.6	1	100.00	21.0	even		ok

Figure S38. Mass Spectrum of **NBD-2FTCF**.

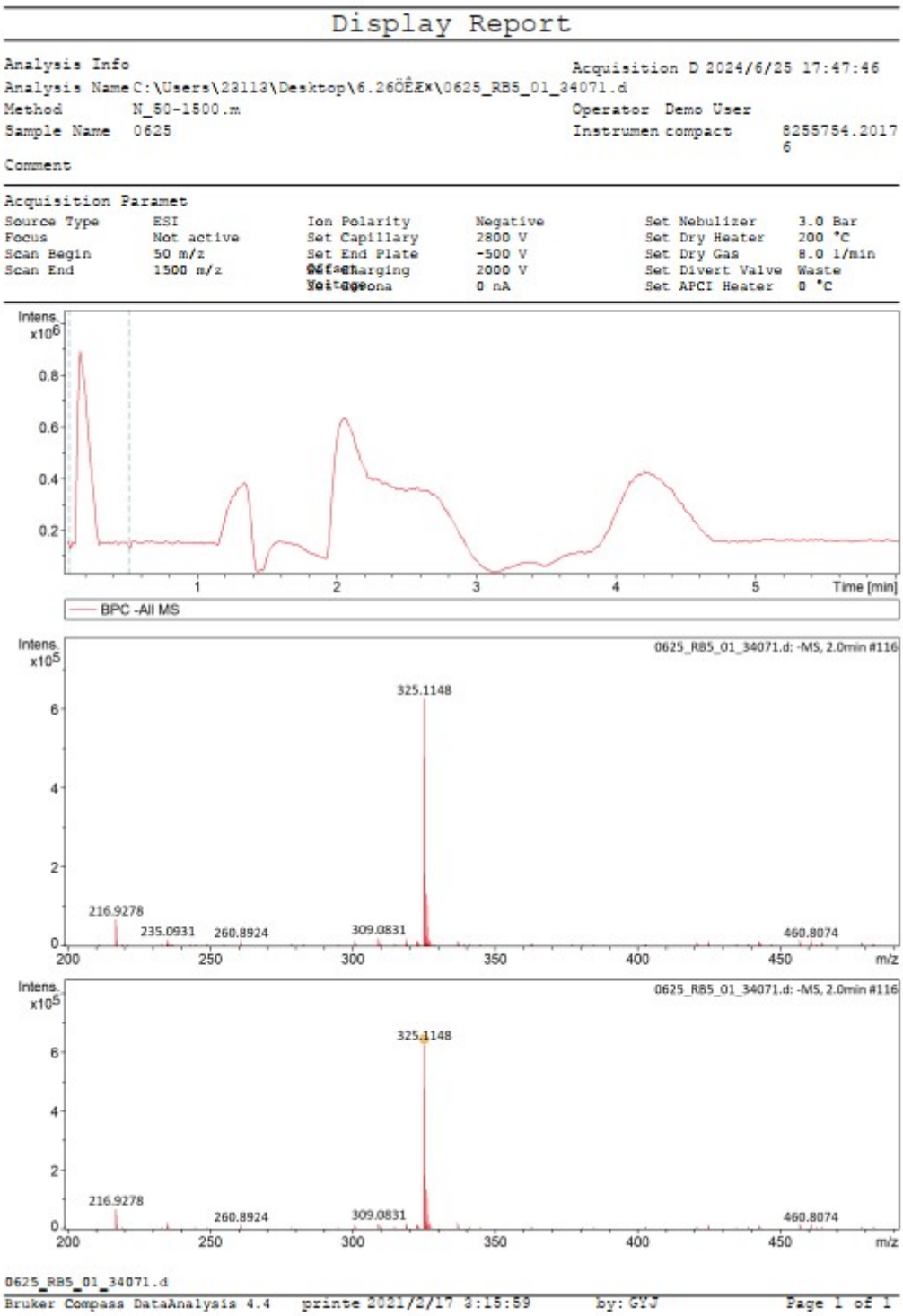

Figure S39. Full HPLC-HRMS spectrum of **2FDCI** with eluted time at 2.0 min and found m/z 325.1148.

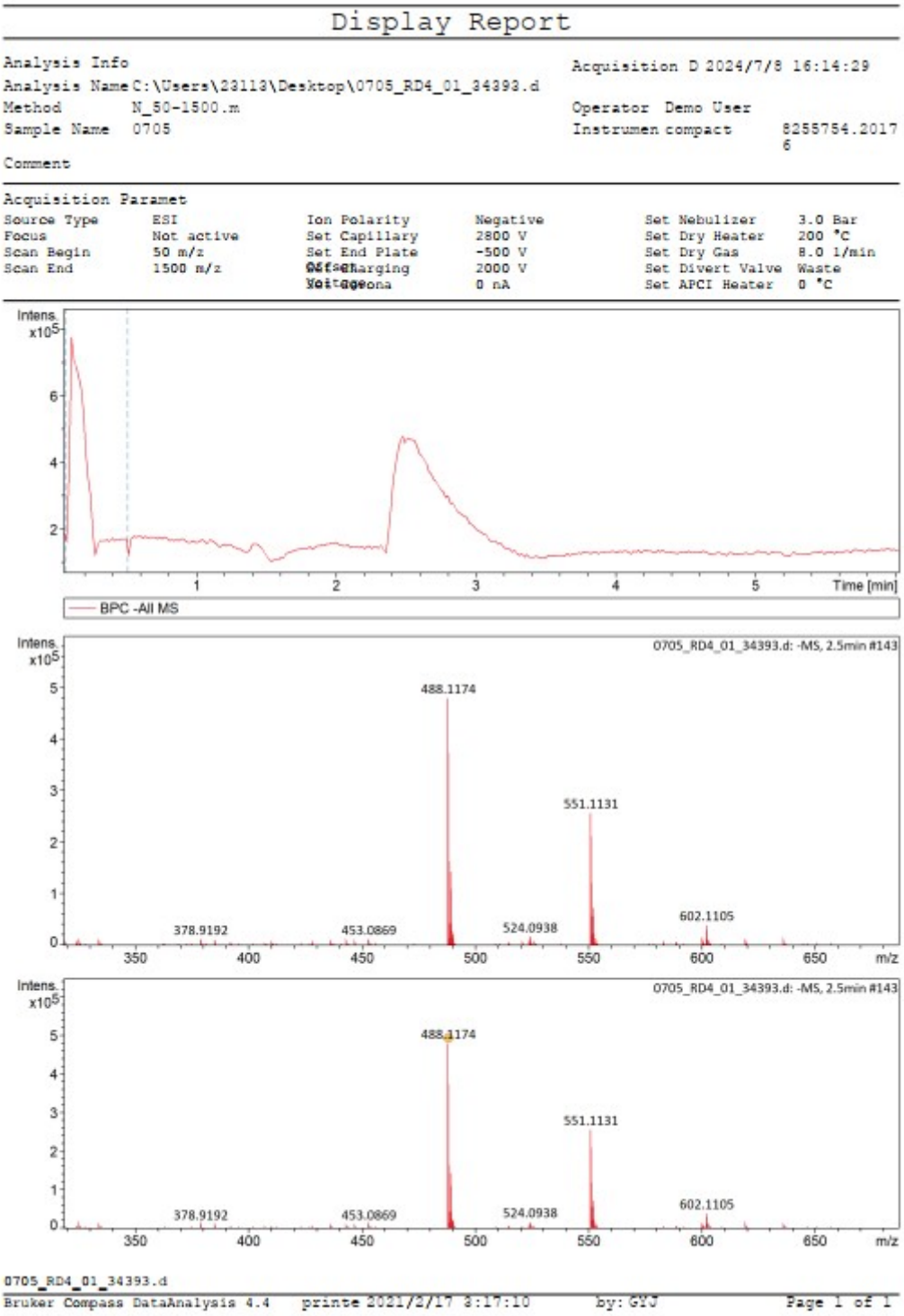

Figure S40. Full HPLC-HRMS spectrum of **NBD-2FDCI** with eluted time at 2.5 min and found m/z 488.1174.

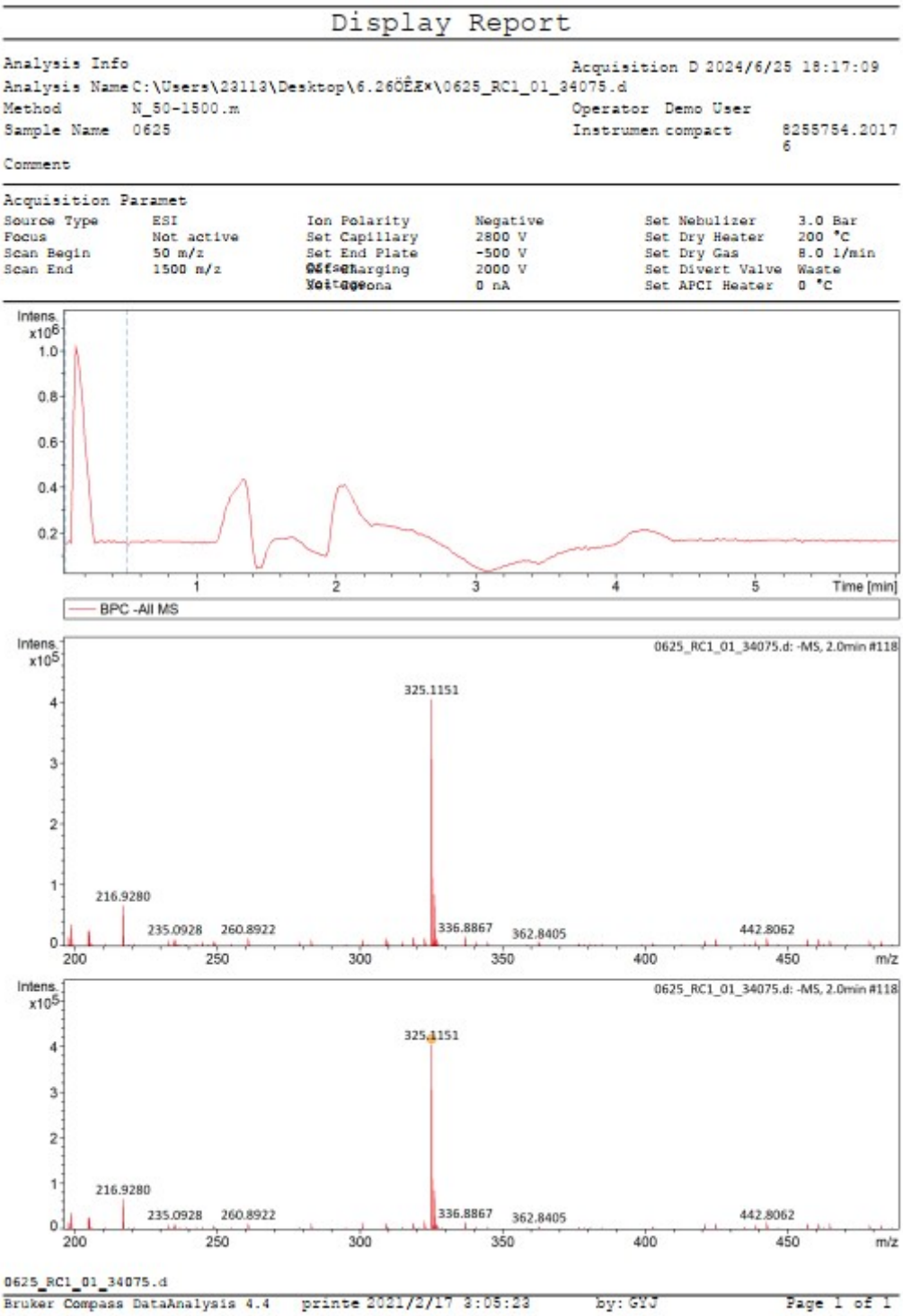

Figure S41. Full HPLC-HRMS spectrum of Cys acted **NBD-2FDCI** with eluted time at 2.0 min and found m/z 325.1151.

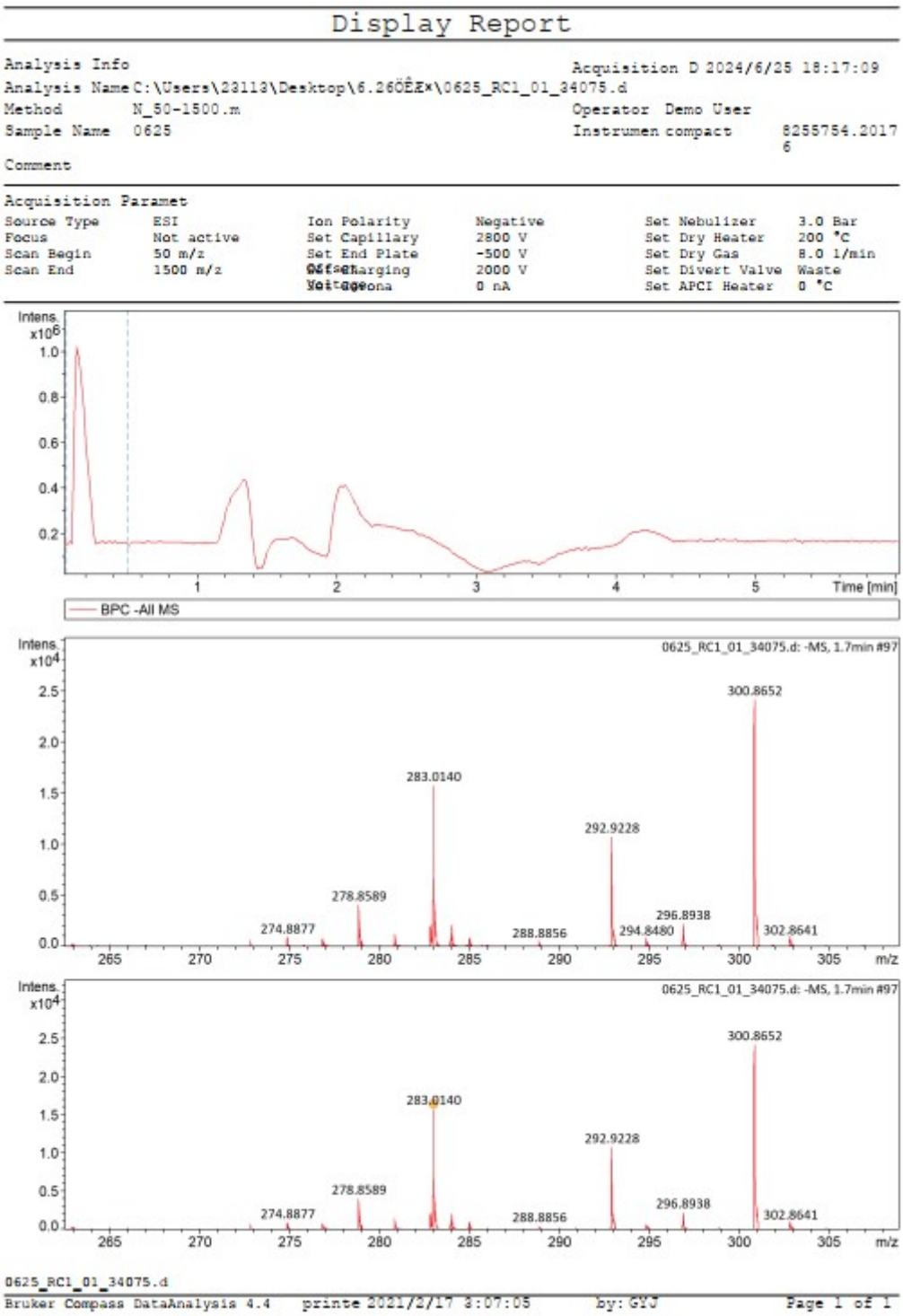

Figure S42. Full HPLC-HRMS spectrum of Cys acted **NBD-2FDCI** with eluted time at 1.7 min and found m/z 283.0140.

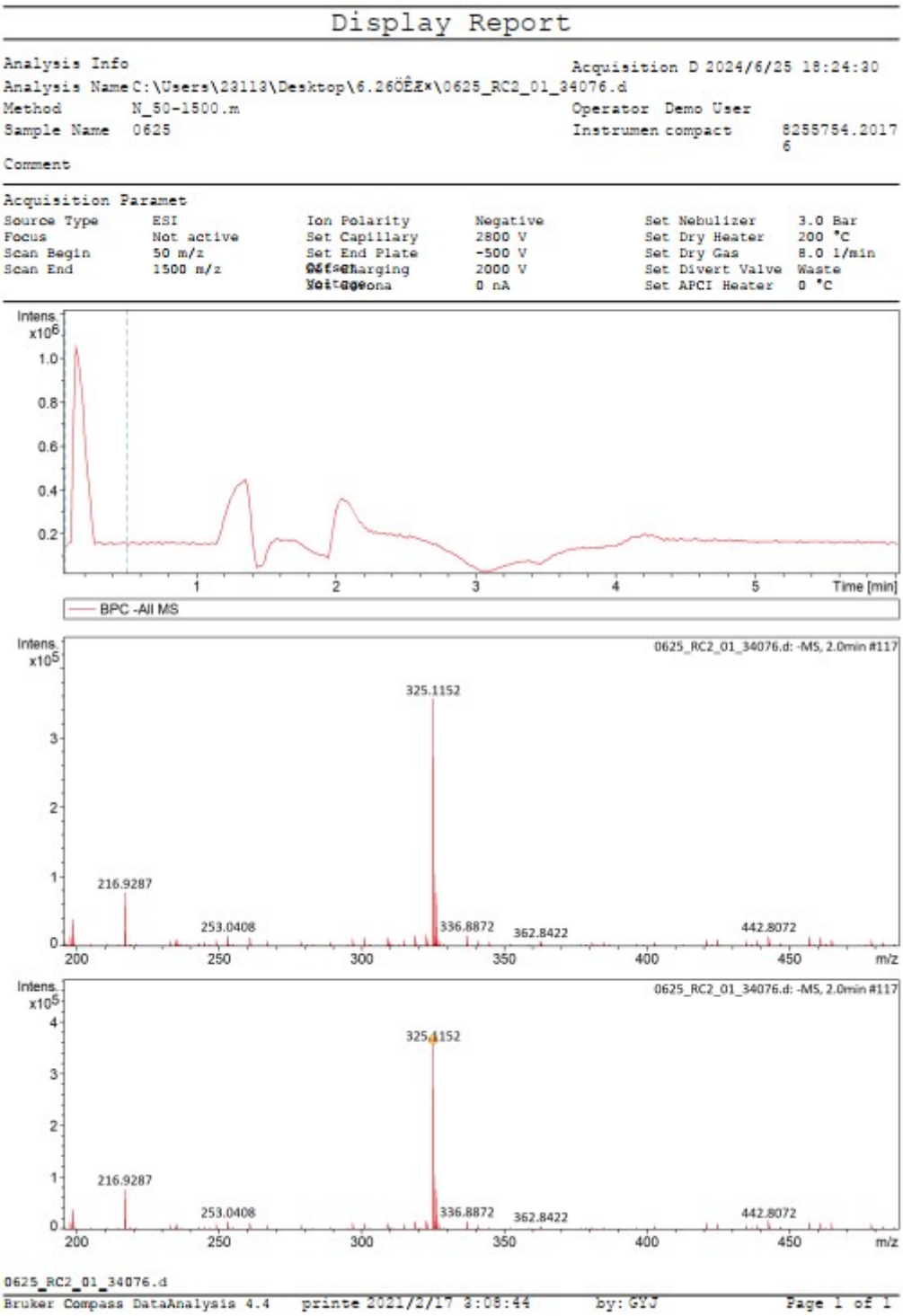

Figure S43. Full HPLC-HRMS spectrum of Hcy acted **NBD-2FDCI** with eluted time at 2.0 min and found m/z 325.1152.

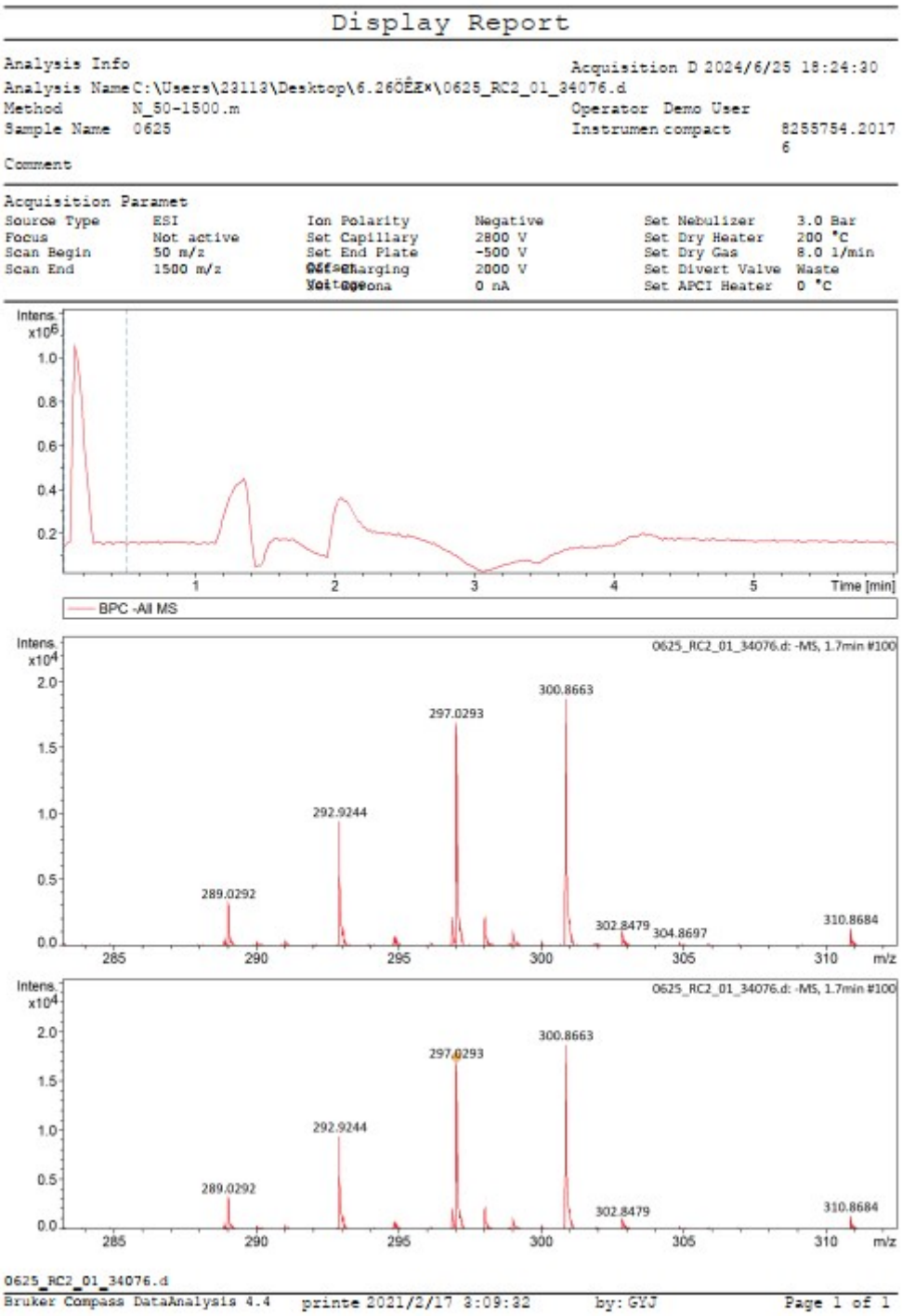

Figure S44. Full HPLC-HRMS spectrum of Cys acted **NBD-2FDCI** with eluted time at 1.7 min and found m/z 297.0293.

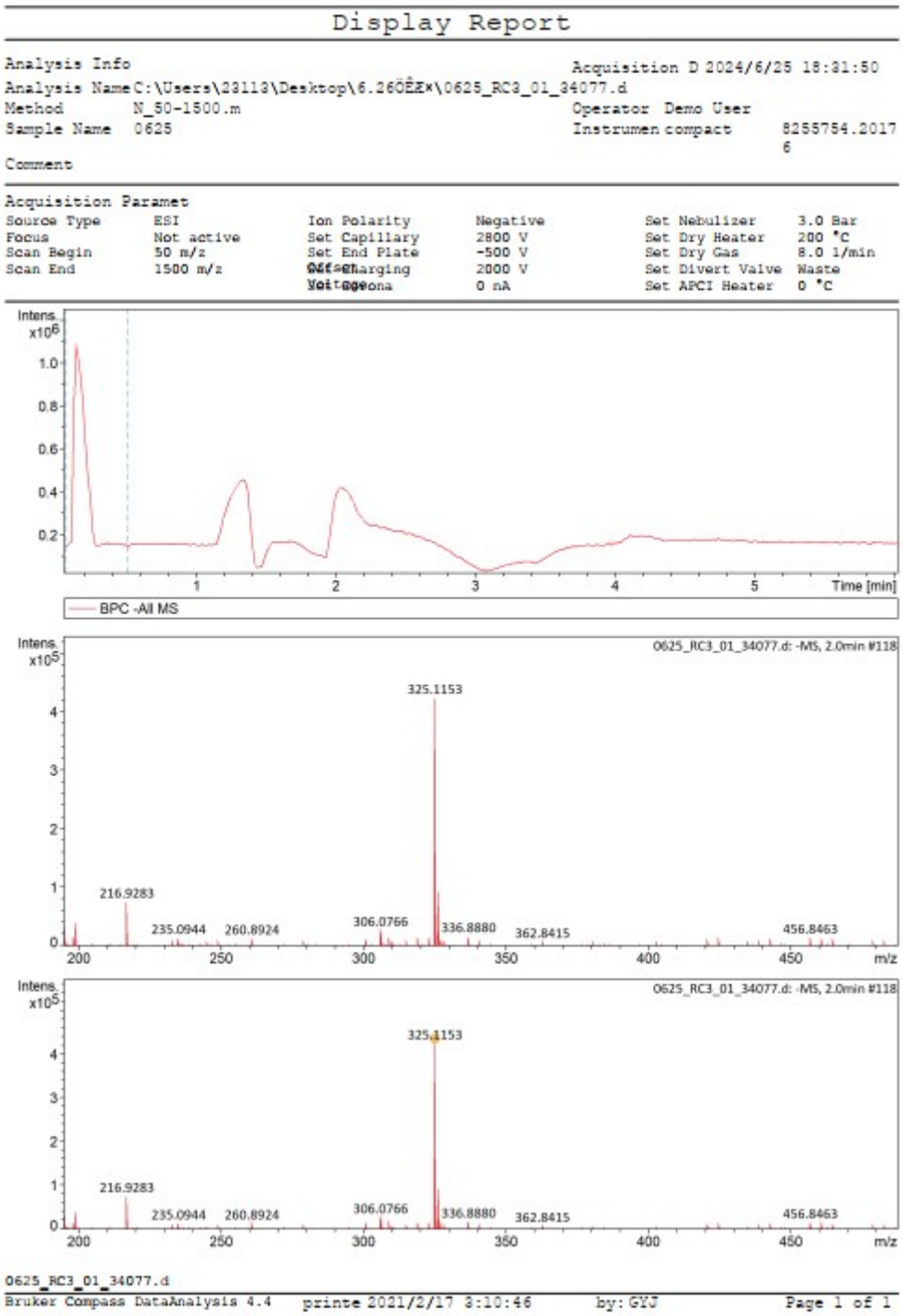

Figure S45. Full HPLC-HRMS spectrum of GSH acted **NBD-2FDCI** with eluted time at 2.0 min and found m/z 325.1153.

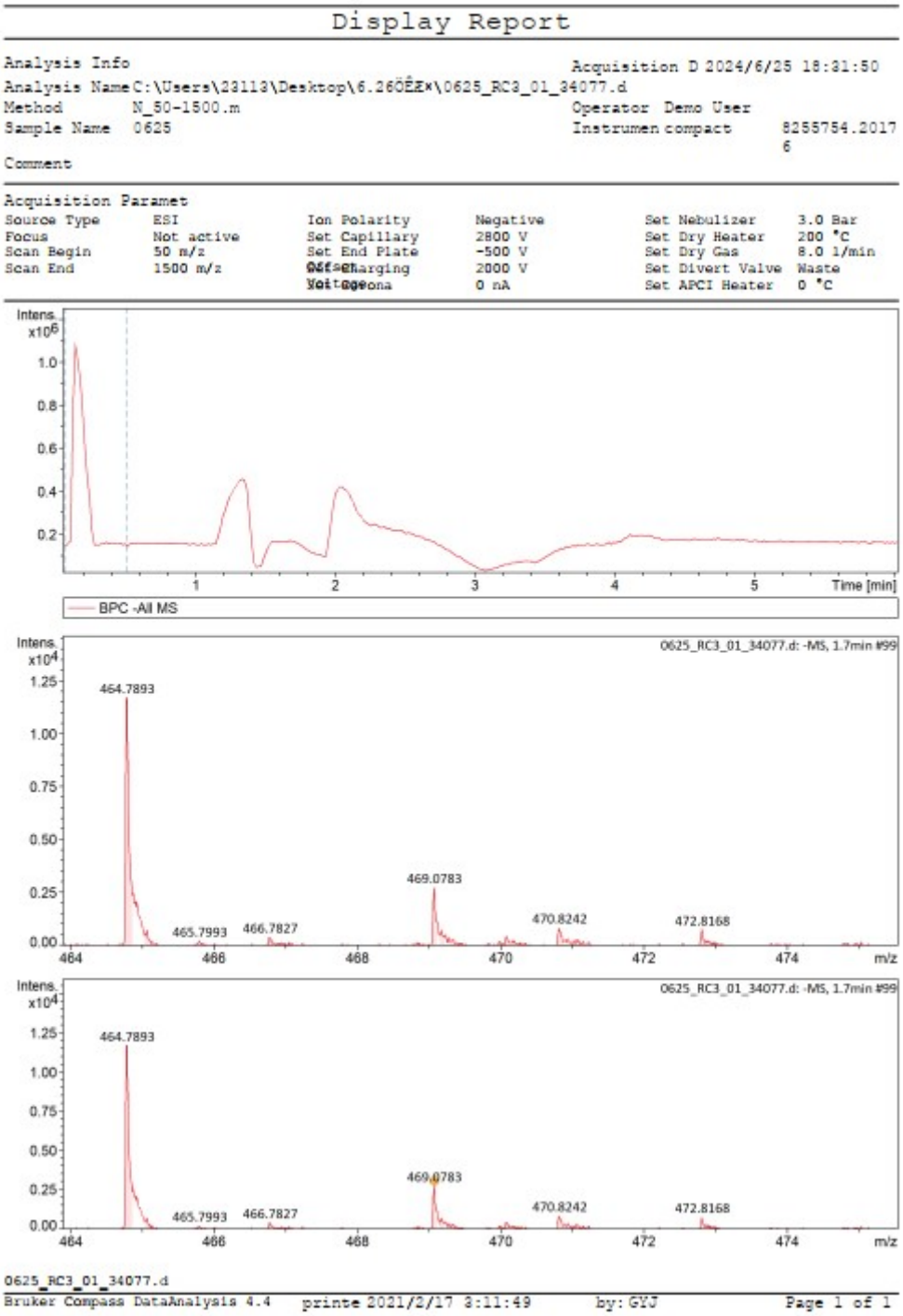

Figure S46. Full HPLC-HRMS spectrum of GSH acted **NBD-2FDCI** with eluted time at 1.7 min and found m/z 469.0783.

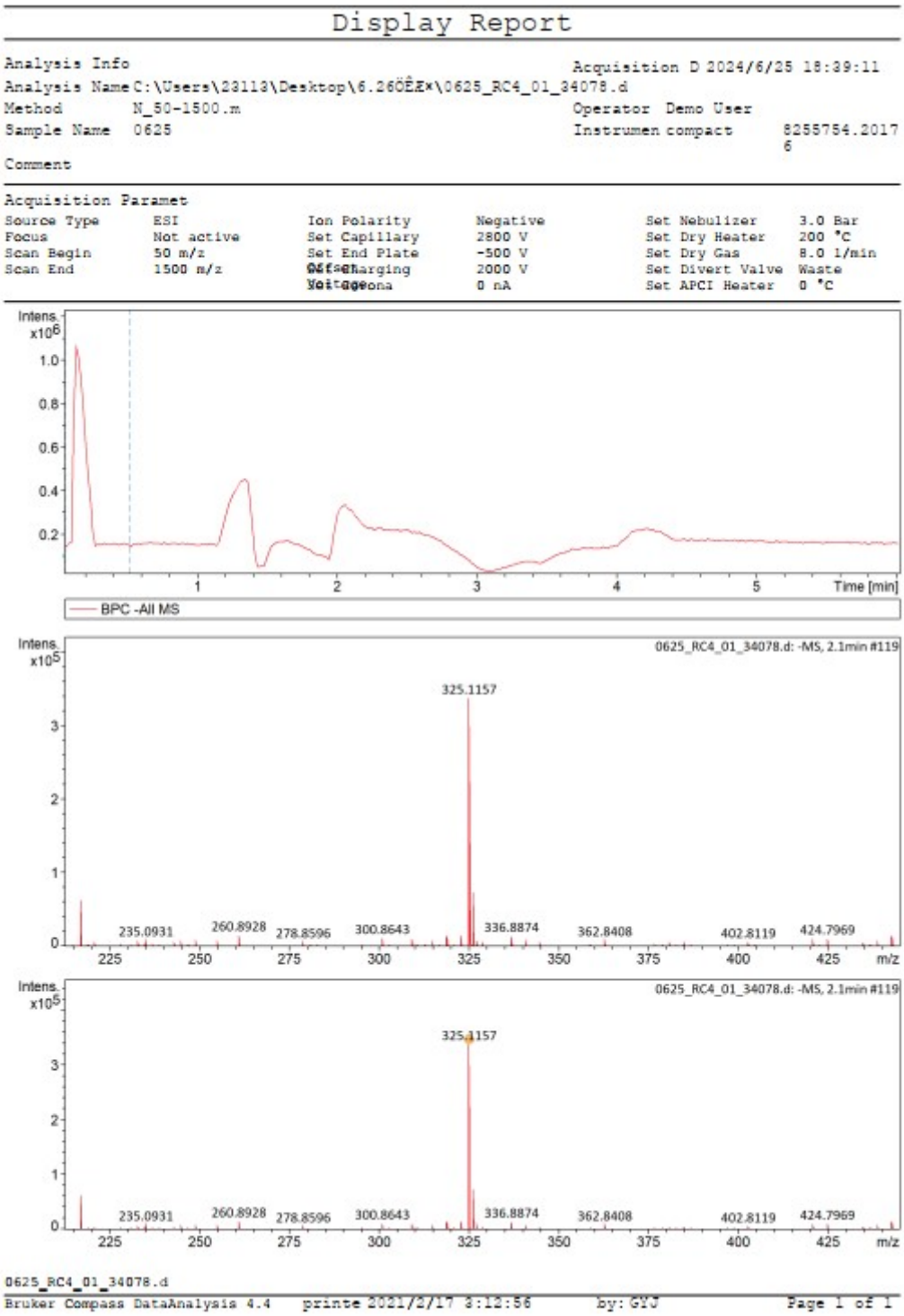

Figure S47. Full HPLC-HRMS spectrum of H_2S acted **NBD-2FDCI** with eluted time at 2.0 min and found m/z 325.1157.

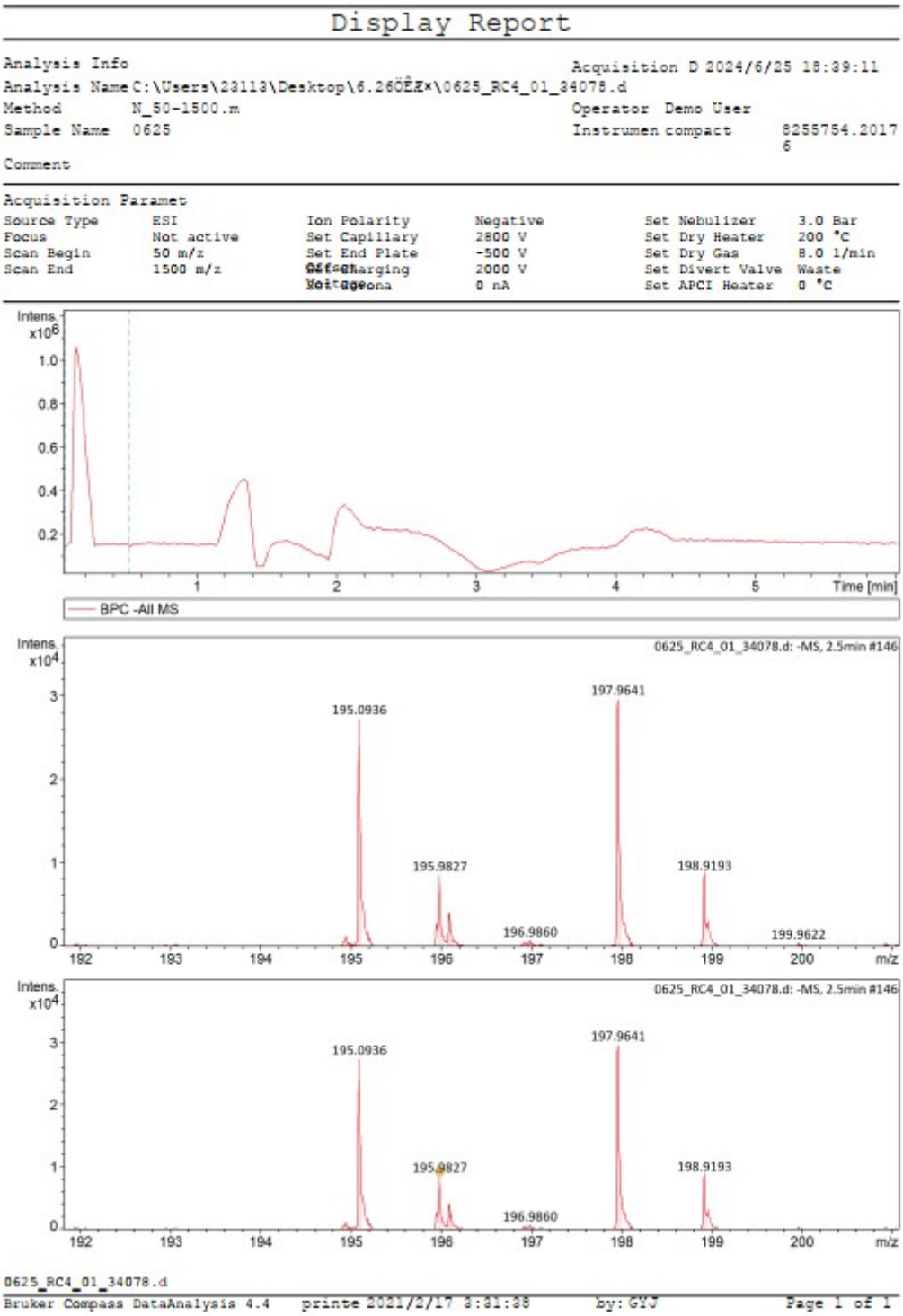

Figure S48. Full HPLC-HRMS spectrum of H_2S acted **NBD-2FDCI** with eluted time at 2.5 min and found m/z 197.9827.